Open access • Posted Content • DOI:10.1101/2021.05.19.444788

The unfolded protein response of the endoplasmic reticulum supports mitochondrial biogenesis by buffering non-imported proteins — Source link

K. Knoeringer, Carina Groh, L. Kraemer, Kevin C. Stein ...+5 more authors

Institutions: Stanford University, Kaiserslautern University of Technology, Harvard University

Published on: 20 May 2021 - bioRxiv (Cold Spring Harbor Laboratory)

Topics: Mitochondrial biogenesis, Inner mitochondrial membrane, Unfolded protein response, Endoplasmic reticulum and Proteostasis

The unfolded protein response of the endoplasmic reticulum supports mitochondrial biogenesis by buffering non-imported proteins

Katharina Knöringer[1]*, Carina Groh[1]*, Lena Krämer[1]*, Kevin C. Stein[2], Katja G. Hansen[3], Johannes M. Herrmann[1], Judith Frydman[2,4], Felix Boos[1,5#]

[1]Cell Biology, Technische Universität Kaiserslautern, 67663 Kaiserslautern, Germany

[2]Department of Biology, Stanford University, Stanford, CA 94305, USA

[3]Department of Genetics, Blavatnik Institute, Harvard Medical School, Boston, MA 02115, USA

[4]Department of Genetics, Stanford University, Stanford, CA 94305, USA

[5]Current address: Department of Genetics, Stanford University, Stanford, CA 94305, USA

*, K.K., C.G. and L.K. contributed equally to this work

#, corresponding author, fboos@stanford.edu

Abstract

Almost all mitochondrial proteins are synthesized in the cytosol and subsequently targeted to mitochondria. The accumulation of non-imported precursor proteins occurring upon mitochondrial dysfunction can challenge cellular protein homeostasis. Here we show that blocking protein translocation into mitochondria results in the accumulation of mitochondrial membrane proteins at the endoplasmic reticulum, thereby triggering the unfolded protein response (UPR^{ER}). Moreover, we find that mitochondrial membrane proteins are also routed to the ER under physiological conditions. The levels of ER-resident mitochondrial precursors is enhanced by import defects as well as metabolic stimuli that increase the expression of mitochondrial proteins. Under such conditions, the UPR^{ER} is crucial to maintain protein homeostasis and cellular fitness. We propose the ER serves as a physiological buffer zone for those mitochondrial precursors that can't be immediately imported into mitochondria while engaging the UPR^{ER} to adjust the ER proteostasis capacity to the extent of precursor accumulation.

Introduction

The ability of cells to maintain protein homeostasis (proteostasis) is crucial for organismal health. Imbalances in protein synthesis, targeting, folding and degradation are associated with numerous diseases and are also hallmarks of aging [1-5]. Cells constantly monitor their proteome to quickly sense proteotoxic perturbations and launch stress-reactive programs to restore homeostasis. Of particular importance are the compartment-specific stress responses to misfolded proteins of the cytosol and nucleus (heat shock response) as well as of the endoplasmic reticulum (unfolded protein response of the ER, UPR^{ER}) and mitochondria (UPR^{mt}). Via the activation of dedicated transcription factors, these pathways elevate the levels of chaperones, proteases and other quality control factors in the compartment where protein misfolding is sensed [6-9].

When misfolded proteins accumulate in the ER, the ER membrane kinase Ire1 dimerizes, autophosphorylates and then splices the mRNA of *XBP1* (*HAC1* in yeast). This enables its efficient translation, giving rise to a potent transcription factor that induces the UPR^{ER} [10]. Besides increasing the expression of ER chaperones and other biogenesis factors, the UPR^{ER} can considerably expand the ER of a cell. In yeast, the Ire1-Hac1 pathway is the only dedicated regulator of the UPR^{ER}, while mammalian cells have two additional branches of the UPR^{ER} that control transcription, translation and eventually apoptosis via PERK and ATF6 [11].

Cellular organelles have clearly distinct organizations and functions, yet they are no independent entities; instead, they form tight physical contacts [12-14] and functionally cooperate in the synthesis of proteins, lipids and metabolites [15,16]. Hence, they mutually influence and rely on the homeostasis of one another. In many protein folding diseases, defects in proteostasis are observed in multiple organelles at the same time, even though the primary perturbation occurs in most cases in only one compartment [17,18]. As a consequence, the different stress response programs need to act in concert [19-23]. For instance, perturbations of mitochondrial proteostasis often compromise mitochondrial protein import so that non-imported precursor proteins accumulate in the cytosol [19,24-26]. Consequently, mitochondrial dysfunction not only activates mitochondrial quality control pathways,

but also the expression of cytosolic chaperones and the ubiquitin-proteasome system, which mitigate the deleterious effects of mistargeted precursors [27-29]. In addition, the synthesis of many mitochondrial proteins is muted by transcriptional repression as well as global translation attenuation to further reduce the burden on cytosolic proteostasis [28,30,31].

While numerous pathways of cross-compartment communication under proteotoxic stress have been identified, our understanding of the connections between organellar stress response programs is still incomplete. Here we show that defective mitochondrial protein import not only activates mitochondrial and cytosolic stress responses, but also triggers the unfolded protein response of the ER. This is at least in part attributable to the targeting of mitochondrial membrane proteins to the ER. The UPR^{ER} is functionally relevant both under conditions of compromised protein import, and conditions that induce mitochondrial biogenesis such as metabolic adaptations. Thus, the UPR^{ER} supports mitochondrial biogenesis by buffering the adverse consequences of elevated levels of non-imported mitochondrial precursor proteins.

Results

The unfolded protein response of the ER is triggered by long-lasting mitoprotein-induced stress

Cellular adaptations to imbalances in mitochondrial proteostasis have been studied using mutants of protein import components [27], chaperones [29], folding-incompetent mitochondrial proteins [31,32], or defects in the respiratory chain [33,34]. Many of these perturbations converge on the impairment of mitochondrial protein import. Model systems in which protein import can be acutely blocked have proven particularly useful to decipher the mechanistic details of responses to such mitoprotein-induced stress. A way of achieving this is the overexpression of mitochondrial precursor proteins that are intrinsically prone to premature folding and stalling inside the narrow mitochondrial translocases [35]. For instance, the well-characterized 'clogger' protein b_2-DHFR can be used for this purpose [28,36]. This fusion protein consists of the N-terminal 167 amino acids of cytochrome b_2 (including its mitochondrial targeting signal) and the rapidly and tightly folding dihydrofolate reductase DHFR (Fig. 1A) [37-39]. Expression of the clogger results in accumulation of non-imported precursor proteins (Fig. 1B) and impairs cell growth (Fig. 1C). In baker's yeast, the expression of b_2-DHFR can be tightly controlled by using a *GAL* promoter that can be switched on by the addition of galactose to the lactate-based growth media. This allows for a tight temporal resolution and the discrimination between short-term and long-term responses to an acute and specific blockade of protein import.

We previously characterized the immediate reactions of the cellular transcriptome to mitoprotein-induced stress [28]. An induction of many chaperones and the proteasome and a repression of OXPHOS components and ribosomes all took place within 1.5 h of clogger expression, some of them even markedly earlier (Fig. 1D). However, many cellular adaptations change when acute stress persists and becomes long-lasting [40-42]. We therefore asked whether cells undergo additional adaptations when exposed to long-term mitoprotein-induced stress. To this end, we reanalyzed our previously collected data to examine changes in the cellular proteome after up to 18 h of clogger

97 expression [28]. We queried for changes in the proteome that were evident at time points no earlier
98 than 4.5 h, which corresponds to approximately one cell doubling in respiratory medium.
99 Interestingly, this criterion identified a group of proteins that are associated with the unfolded
100 protein response of the ER (Fig. 1E and S1A) [21]. Some individual targets of the UPR^{ER}, such as e.g.
101 Ero1 and Kar2, were induced at earlier time points, presumably due to their responsiveness to the
102 transcription factors Hsf1 and/or Rpn4 that form the first line of defense against mitoprotein-
103 induced stress. Moreover, a small number of UPR targets were decreased over time. These proteins
104 (Hem15, Mdl1, Coq6, Mgr1) almost exclusively localize to mitochondria and their levels are likely
105 affected by the import block or the clogger-induced downregulation of mitochondrial components.
106 However, most UPR targets showed a consistent upregulation that was observed 9 h after clogger
107 induction, and even more so after 18 h (Fig. 1E and S1A).

108 In yeast, the UPR^{ER} is activated by splicing of an intron from the *HAC1* mRNA in the cytosol
109 through the ER-resident kinase Ire1. Only the spliced isoform of the mRNA (called *HAC1*^{i}) can be
110 translated and gives rise to a transcription factor [10]. To test whether *HAC1* was indeed spliced and
111 translated under mitoprotein-induced stress, we analyzed clogger-expressing cells by ribosome
112 profiling. Here, ribosome footprints from cells expressing b_2-DHFR or cytosolic DHFR were
113 sequenced 4.5 h after induction, and the changes in the translatome were compared to the changes
114 in the transcriptome (Fig. 1F). For the large majority of all genes, transcriptional and translational
115 changes correlated tightly. For *HAC1* however, we observed a slight reduction of mRNA levels,
116 while we found four times more ribosome footprints on *HAC1* mRNA in clogger-expressing than in
117 control cells (Fig 1G). In fact, *HAC1* was one of the most prominent outliers in this comparison,
118 ranking as the gene with the second-highest gain in translational efficiency when mitochondrial
119 import was blocked (Fig. S1B). The increase in ribosome occupancy was restricted to the exon
120 region of the mRNA, while the intron region of *HAC1* was free of ribosome densities in both
121 conditions (Fig 1H).

We next sought to more precisely determine the timing of the UPR^{ER} activation. To this end, we set up an RT-qPCR assay which quantifies the spliced isoform of *HAC1*^{i} by using a primer-probe combination which specifically recognizes the exon-exon junction of *HAC1*^{i} (Fig. S1C, D). We induced b_2-DHFR by addition of 0.5% galactose to cultures that were previously grown in lactate medium and followed *HAC1* splicing over time. The earliest time point at which we could detect a considerable difference between clogger-expressing and control cells was 3 h (Fig. 1I). As a certain delay between the onset of *HAC1* splicing and downstream changes in protein levels of UPR^{ER} targets is expected, this is consistent with our earlier observation that UPR^{ER} induction is a rather late event in mitoprotein-induced stress signaling.

We conclude that under long-term impairment of mitochondrial protein import, cells induce the UPR^{ER} via the canonical Ire1-Hac1 pathway.

UPR^{ER} induction is required for cellular fitness under mitoprotein-induced stress

We asked whether UPR^{ER} induction is functionally relevant under sustained mitoprotein-induced stress, given that its magnitude is rather mild when compared to harsh ER insults such as treatment with tunicamycin (*cf.* Fig. S1C). To this end, we compared the fitness of UPR^{ER}-deficient cells with that of wild type cells when mitochondrial import was blocked. Indeed, when either *HAC1* or *IRE1* were deleted, cells exhibited synthetic growth defects upon clogger expression, both in liquid medium and on plates (Fig. 2A, B).

We examined the relevance of UPR^{ER} signaling when mitochondrial import is impaired by an approach orthogonal to clogging the translocases. To this end, we deleted *HAC1* or *IRE1* in a strain that carries a temperature-sensitive mutation in the essential import component Mia40. Mia40 is responsible for the import and oxidative folding of cysteine-containing mitochondrial intermembrane space proteins [43,44]. The import defects in the *mia40-4* mutant were shown to trigger cytosolic adaptations (unfolded protein response activated by mistargeting of proteins, UPR^{am})

147 similar to those elicited by the clogger [27]. Indeed, *mia40-4* cells grew worse at semi-permissive
148 growth conditions when *IRE1* or *HAC1* were deleted, demonstrating that UPR^{ER} signaling is
149 relevant when protein import into the IMS is perturbed (Fig. 2C).

150 In conclusion, defects in mitochondrial protein import trigger the UPR^{ER}, which is required for
151 cellular fitness under such conditions (Fig. 2D).

152

153 **Mitochondrial membrane proteins accumulate at the ER when mitochondrial protein import**
154 **is impaired**

155 What could be the cause for UPR^{ER} activation in situations when mitochondrial import is impaired?
156 Blocking import should elevate levels of mitochondrial precursor proteins in the cytosol. Therefore,
157 we reasoned that a portion of these non-imported precursors, perhaps comprising membrane
158 proteins, may be targeted to the ER, where they would accumulate and engage folding and protein
159 quality control systems, thus triggering UPR^{ER} activation.

160 To test this hypothesis, we labelled the mitochondrial inner membrane protein Oxa1 with
161 ymNeonGreen, and coexpressed it with Sec63-ymScarletI as an ER marker, followed by analysis of
162 their subcellular distribution by fluorescence microscopy. When we expressed cytosolic DHFR, the
163 green Oxa1 signal and the red Sec63 signal partitioned into separate structures with no considerable
164 colocalization. In contrast, when b_2-DHFR was expressed for 4.5 h, we found that a fraction of
165 Oxa1-ymNeonGreen colocalized with Sec63-ymScarletI in the typical ring-shaped structures of the
166 perinuclear and peripheral ER (Fig. 3A). This ER co-localization was observed in around 30% of
167 the clogger-expressing cells, but only in around 1% of control cells (Fig. 3B).

168 Fusions with fluorescent proteins can interfere with the function, localization, folding and stability
169 of proteins [45-47]. In particular, a large, stably folding C-terminal moiety might generate a
170 mitochondrial clogger, as exemplified by b_2-DHFR itself, and interfere with import and
171 localization. We therefore sought to verify our results by a method that avoids the fusion of large

protein domains to mitochondrial precursors and also minimizes the need for manual categorization of microscopic images with high mitochondrial background signal. To this end, we adapted a split-GFP method specifically designed to assess protein localization *in vivo* [48]. Superfolder GFP is split into two parts, GFP^{1-10} and GFP^{11}, which only emit fluorescence when co-localized to the same compartment (Fig. 3C). The GFP fragments do not alter the folding behavior of the fusion proteins and their affinity is high enough to promote self-association without the need for a direct protein-protein interaction of the fusion partners [49-51]. The GFP^{11} tag consists of only 17 amino acid residues and is therefore unlikely to affect translocation across the mitochondrial membranes.

To first verify that the split-GFP assay captures the subcellular localization of mitochondrial proteins, we fused the GFP^{11} fragment to the C-terminus of Oxa1 (inner membrane, C-terminus at matrix side), Mia40, Dld1 (inner membrane, C-terminus at IMS side) and Om45 (outer membrane, C-terminus at IMS side) and the GFP^{1-10} fragment to Oxa1 (IM, matrix side), Mia40 (IM, IMS side), Sec63 (ER membrane, cytosolic side) and Ssa1 (cytosol) (Fig. S2A) [52-58]. In the absence of any stress, the by far strongest fluorescence signal was detected for the combinations that recapitulate the known localization and topology for all proteins tested (Oxa1-GFP^{11} / Oxa1-GFP^{1-10}, Mia40-GFP^{11} / Mia40-GFP^{1-10}, Dld1-GFP^{11} / Mia40-GFP^{1-10}, Om45-GFP^{11} / Mia40-GFP^{1-10}), while all other combinations resulted in much lower fluorescent signals (Fig. 3D and S2B-D, control condition in blue). This showed that the approach can measure protein localization with sub-organellar resolution.

We next expressed either b_2-DHFR or cytosolic DHFR for 4.5 h in strains carrying the split-GFP reporters. b_2-DHFR expression evoked a marked increase in signal for Oxa1-GFP^{11} with the Sec63-GFP^{1-10} and the Ssa1-GFP^{1-10} reporters, while with cytosolic DHFR, only very little signal was detected (Fig. 3D). This points towards relocation of a fraction of newly synthesized Oxa1-GFP^{11} to the ER surface or, potentially, the cytosol. We used fluorescence microscopy to confirm that the fluorescence we measured in a plate reader setup indeed originated from ER-localized GFP complementation (Fig. 3E and S2E-F). For the mitochondrial outer membrane protein Om45-

GFP^{11}, we found a similar redistribution to the ER under import stress (Fig. 3F and S2B), while neither Mia40-GFP^{11} nor Dld1-GFP^{11} showed detectable ER localization (Fig. S2C, D). Obviously, some but not all mitochondrial membrane proteins are routed to the ER when their entry into mitochondria is delayed.

How is the timing of precursor localization to the ER after mitochondrial import is blocked? To assess this question, we grew cells expressing Oxa1-GFP^{11} and Sec63-GFP$^{1-10}$ in a plate reader, induced b_2-DHFR or cytosolic DHFR by addition of galactose and monitored split-GFP fluorescence over time in living cells. Constitutively expressed ymScarletI was used to normalize for differences in cell growth and translation rates. Clogger-expressing cells showed elevated split-GFP signals from around 3 h after induction (Fig. 3G). Strikingly, the induction of the UPR^{ER} and the detection of Oxa1 at the ER perfectly coincided in time (*cf.* Fig. 1I).

In conclusion, when mitochondrial import is blocked, some mitochondrial preproteins accumulate at the ER membrane which likely evokes the UPR^{ER} (Fig. 3H).

The UPR^{ER} maintains cellular fitness during adaptation of mitochondrial biogenesis

Is the UPR^{ER} only a stress-reactive system that comes into play when mitochondrial import is defective, or is it of more general relevance for mitochondrial biogenesis? Accurate protein sorting is a challenging task for cells, and the ER might constantly encounter a certain load of mitochondrial precursor proteins. To check whether there is evidence for mitochondrial proteins routed to the ER in the absence of stress, we reanalyzed several high-resolution datasets on protein targeting. Proximity labeling of ribosomes close to the ER or the mitochondrial outer membrane and subsequent ribosome profiling determined the 'local translatome' at the ER and mitochondrial surface in yeast [59,60]. Interestingly, while most mitochondrial proteins were enriched in the vicinity of mitochondria, a subset of mitochondrial proteins was found to be translated close to the ER, notably including Oxa1 (Fig. 4A). Also in human cells, mRNAs of some mitochondrial proteins

were found at the ER surface (Fig. S3A) [61]. Finally, we reanalyzed datasets from studies that determined which nascent chains interact with the signal recognition particle (SRP) in yeast by pulldown of SRP and subsequent sequencing of the bound transcripts [62,63]. SRP is a major targeting factor for secretory proteins that carry a signal sequence or transmembrane domains [64-67]. While secretory proteins were clearly the most enriched among the SRP substrates, a subset of mitochondrial encoding ribosome-nascent chains were also bound by SRP to a lesser extent, but significantly above what was found for cytosolic proteins (Fig. S3B). Both in yeast and in human cells, ER-localized mitochondrial transcripts include, but are not limited to proteins with known dual localization to mitochondria and ER. Apparently, some mitochondrial precursors have a tendency to be targeted to the ER even in the absence of stress, possibly mediated by 'low priority' SRP-binding to at least some of these precursors.

We did not observe considerable fluorescence in our split-GFP assays without applying import stress. However, under steady state conditions, precursors might only very transiently localize to the ER because they can be efficiently rerouted to mitochondria with the help of the ER-resident J protein Djp1 in a process called ER-SURF [15]. Loss of this pathway does not impair mitochondrial import *per se*, but would trap mitochondrial orphans at the ER. To test this, we employed our split-GFP assay in the 'ER-trapping' Δ*djp1* mutant and found accumulation of Oxa1 at the ER even under optimal growth conditions (Fig. 4B). Hence, there is indeed a constitutive flux of mitochondrial precursors to the ER in the absence of stress.

We therefore wondered whether the UPR^{ER} might be required to buffer fluctuations in the levels of ER-localized mitochondrial precursors under physiological conditions. Mitochondrial biogenesis is strongly dependent on the carbon source in the growth media: The levels and, hence, synthesis of many mitochondrial proteins are low on glucose, but considerably higher on raffinose, galactose, glycerol or lactate [68-70]. In fact, we observed that the extent of steady state *HAC1* splicing was low when cells were grown on glucose, but elevated on all other carbon sources, particularly on galactose and glycerol (Fig. 4C). To assess the functional relevance of the UPR^{ER} under different

states of mitochondrial metabolism, we grew wild type, Δ*hac1* and Δ*ire1* cells to exponential phase in liquid medium containing glucose, galactose or lactate as sole carbon source. Then we washed the cells, resuspended them in glucose, galactose and lactate medium in all possible combinations and monitored their growth (Fig. 4D). While there was no difference between wild type and ER-deficient strains when they remained in the media they were cultured in before, Δ*hac1* and Δ*ire1* mutants had problems to adapt when carbon sources were switched to a medium with higher levels of *HAC1* splicing. Likewise, ER-deficient strains grew well during exponential phase in glucose, but exhibited a phenotype at high optical densities, shortly before the cultures entered the stationary phase. At this point, yeast cells respond to the depletion of glucose and switch to respiratory metabolism, a growth phase called diauxic shift in which mitochondrial biogenesis is strongly induced [71,72]. Hence, the UPR^{ER} is important when such a remodeling takes place.

Would a stronger UPR^{ER} help cells to adapt to respiratory growth conditions? Yeast cells grew better on respiratory media when exposed to moderate amounts of the reducing agent dithiothreitol (DTT), which is a known trigger of the UPR^{ER} and, consequently, is toxic for UPR-deficient strains (Fig. 4E). However, its beneficial effect on respiratory growth might – at least in part – also result from UPR^{ER}-independent effects. We therefore sought to induce the UPR^{ER} directly without any stress treatment by expressing the spliced isoform of *HAC1* from a β-estradiol-inducible *GAL* promoter [23]. Cells were precultured in glucose medium and, upon shift to either glucose or lactate medium, exposed to various β-estradiol concentrations, i.e. to different levels of *HAC1*^{i} expression. Indeed, cells grew better in lactate when *GAL-HAC1*^{i} was induced with up to 50 nM β-estradiol, while they were not affected when grown in glucose (Fig. 4F). Higher concentrations of β-estradiol delayed growth, consistent with earlier reports that overshooting UPR^{ER} activation can be toxic [73,74].

Obviously, a functional UPR^{ER} is not only important when mitochondrial protein import is blocked, but also maintains cellular fitness under physiological conditions with elevated mitochondrial biogenesis. We propose that a fraction of mitochondrial precursor proteins is always localizing to the ER, either transiently as part of the ER-SURF pathway or terminally mistargeted. When the

275 influx of precursors is altered due to changes in gene expression or by mitochondrial dysfunction,
276 the UPR^{ER} acts as a 'rheostat' and adjusts the protein folding and quality control components of the
277 ER accordingly (Fig. 4G).

278

Discussion

Precursor proteins that accumulate outside mitochondria impose a burden on cellular proteostasis. Many precursors remain in the cytosol [31] or end up in the nucleus [75], where chaperones and the proteasome mitigate the adverse effects of mistargeted proteins and eventually degrade them [27,28,76,77]. Membrane proteins are particularly prone to misfolding and aggregation in an aqueous environment. Hence, their prolonged presence in the cytosol can be very hazardous for cells [78,79]. We found in this study that cells can adsorb precursors of mitochondrial membrane proteins to the surface of the ER and employ the UPR^{ER} to buffer their elevated levels at the ER. Apparently, mitochondrial proteins associate with the ER even under physiological conditions. However, the accumulation of mitochondrial precursors at the ER is exacerbated by import defects as well as by metabolic stimuli that increase the expression of abundant mitochondrial enzymes, many of which are membrane proteins. Our observations identify the UPR^{ER} as an important cellular response to promote cellular fitness under such conditions, especially during the phase of adaptation.

There are numerous reasons why engaging the ER as a venue for buffering mitochondrial membrane proteins can be beneficial: (1) The large ER membrane provides a favorable environment for proteins with hydrophobic transmembrane domains that would otherwise misfold in the aqueous cytosol. (2) The ER has a remarkable capacity to prevent protein aggregation, even exceeding that of the cytosol for some classes of proteins [80,81]. (3) Besides having chaperones that promote protein folding, the ER harbors an elaborate machinery for ER-associated protein degradation (ERAD). ER components have been found to participate in the degradation of cytosolic and, more recently, mitochondrial proteins [82,83]. (4) ER and mitochondria share many components in their protein biogenesis and quality control systems, e.g. the Hsp40 co-chaperone Ydj1 or Cdc48/VCP/p97 and many of its cofactors [36,84-86]. In addition, some organelle-specific factors of ER and mitochondria physically interact and functionally cooperate with each other [87]. (5) Protein transfer between mitochondrial and ER membranes is possible via dedicated machineries that can extract mislocalized proteins from the membrane and set them back en route to the respective other

organelle [15,88-91]. (6) The close proximity of mitochondria and ER at membrane contact sites might facilitate the exchange of proteins between the two organelles. Interestingly, ER-mitochondria contact sites are enriched with ER chaperones and other UPR^{ER} effectors [92] and their loss activates the UPR^{ER} [93]. In addition, contact sites are crucial for the initiation of autophagy [94,95].

Based on the above considerations, it is possible that routing of mitochondrial precursors to the ER could be more than a mere 'mistake' in protein targeting, but rather an actively regulated quality control pathway. In line with this idea, our analyses show that SRP recognizes and binds nascent chains of some mitochondrial proteins, suggesting that a portion of the mitochondrial proteome is synthesized at the ER surface. Also the GET pathway (guided entry of tail-anchored proteins) was recently identified to be involved in ER targeting of mitochondrial tail-anchored proteins and some carrier proteins [88,96].

Our findings add to a significant body of observations linking the stress responses and homeostasis mechanisms of mitochondria and ER [97]. Several processes connect mitochondrial and ER homeostasis in the context of stress: the flux of lipids between mitochondrial and ER membranes [98]; the generation of ATP as well as reactive oxygen species by the respiratory chain [99,100]; the transport of calcium [16,101]; or the availability of building blocks for glycosylation of secretory proteins, provided by mitochondrial carbohydrate metabolism [102]. We propose that mitochondria and ER are also linked in the management of mitochondrial biogenesis.

Our findings open the question which of the many components and pathways that are reinforced by the UPR^{ER} are the most important for the management of ER-localized mitochondrial proteins. It will be exciting to disentangle the exact contributions of storage and handling of misfolding-prone precursors, their transfer to mitochondria or their degradation at the ER surface.

We suggest that cells engage the ER and its proteostasis capacity – augmented by the UPR^{ER} when necessary – as a buffer for proteins that can't be immediately imported into mitochondria. From there, they can be either degraded or kept on hold for a second attempt of mitochondrial import.

Therefore, we should consider to rethink the classical concept of 'mislocalization' as a problem that cells need to avoid. Rather, spatial sequestration (transient or terminal) of proteins to compartments other than those they are primarily targeted to might be a productive step in protein biogenesis. It will be exciting to explore this concept and the components that are involved in the future.

Materials and Methods

Yeast strains and plasmids

All yeast strains used in this study are listed in Supplementary Table S1 and were based on the wild type strain W303 or YPH499 [103,104]. The *mia40-4* strain was a gift from Agnieszka Chacinska [44]. Yeast strains were grown on YP medium (1% yeast extract, 2% peptone) or synthetic medium (0.17% yeast nitrogen base and 0.5% $(NH_4)_2SO_4$) containing 2% glucose, 2% galactose, 2% raffinose, 2% glycerol or 2% lactate and supplemented with appropriate amounts of amino acids and nucleobases for selection.

pFA6a-ymNeongreen-*CaURA3* and pFA6a-ymScarletI-*CaURA3* were kindly provided by Bas Teusink (Addgene plasmids # 125703 and # 118457) [105]. Genomic tagging with ymNeonGreen was performed by amplifying the ym-NeonGreen-CaURA3 cassette with overhangs homologous to the *OXA1* locus and transforming yeast cells using the lithium acetate/ss carrier DNA/PEG method [106]. Genomic deletion of *IRE1* and *HAC1* in the *mia40-4* background was performed by amplifying a kanMX4 cassette from a pFA6a plasmid with overhangs homologous to the sequences up- and downstream of the genomic open reading frames of the target genes [106]. Yeast cells were transformed with the PCR product and grown on plates containing 150 µg/ml G418 for selection. Deletions were confirmed by colony PCR on the targeted genomic loci.

The sequences of GFP^{11} (pSJ1321, pRS315-NOP1pr-GFP11-mCherry-PUS1) and GFP^{1-10} (pSJ2039, pRS316-NOP1pr-GFP1-10-SCS2TM) were a gift from Sue Jaspersen (Addgene plasmids # 86413 and # 86418) [48]. Cloning of the split-GFP constructs into the pYX122, pYX142 and pNH605 plasmids used in this study was performed by Gibson Assembly with the HiFi DNA Assembly Master Mix (New England Biolabs, #E2621L) according to the manufacturer's instructions. The GFP^{11} part was fused to the different proteins by integration of the sequence (5' AGA GAT CAT ATG GTT TTG CAT GAA TAT GTT AAT GCT GCT GGT ATT ACT TAA 3') into the corresponding primers. GFP^{1-10} was amplified from the plasmid (pSJ2039) with overhangs homologous to the end of the fusion partner and the plasmid pYX122.

363 **Isolation of RNA and RT-qPCR**

364 RNA was extracted from yeast cells using either the acid phenol-chloroform method or an RNeasy
365 Mini kit with on-column removal of DNA (Qiagen), both as previously described [28]. In either case,
366 3 OD_{600}×ml of cells were collected by centrifugation (17,000 × *g*, 3 min, 2°C), washed with
367 prechilled water, snap-frozen in liquid nitrogen and stored at -80°C.
368 For acid phenol-chloroform extraction, cell lysates were prepared in lysis buffer (50 mM Tris/HCl
369 (pH 7.0), 130 mM NaCl, 5 mM EDTA, 5% (w/v) SDS) with a FastPrep-24 5 G homogenizer (MP
370 Biomedicals) with 3 cycles of 20 s, speed 6.0 m s^{-1}, 120 s breaks, lysis matrix Y). RNA was
371 purified with repeated extraction with acid phenol–chloroform (5:1, pH 4.5, two times) and 24:1
372 chloroform–isoamylalcohol (24:1). Then, 0.3 M sodium acetate (pH 5.5) was added, RNA was
373 precipitated with ethanol and solubilized in water. DNA was removed using a Turbo DNA Free kit
374 (Ambion) following the manufacturer's instructions. RNA purity and concentration were assessed
375 using a DeNovix DS-11 FX+ Fluorometer.
376 RT-qPCR was performed with a CFX96 Touch Real-Time PCR Detection System (Bio-Rad). 100
377 ng total RNA per 20 µl reaction were analyzed using the Luna Universal Probe One-Step RT-qPCR
378 Kit (NEB, # E3006) in technical triplicates. cDNA was generated by reverse transcription for 10
379 min at 55°C. PCR amplification was then carried out under the following conditions: initial
380 denaturation for 1 min at 95°C, followed by 45 cycles of 10 s at 95°C (denaturation) and 30 s at
381 60°C (extension). Primer-probe combinations for qPCR are listed in Supplementary Table 3. For
382 the specific detection of the spliced isoform of *HAC1*, primers were chosen to flank the intron and
383 the fluorescent probe spans the exon-exon junction (Fig. S1B). Primer efficiency was determined by
384 measuring serial dilutions of pooled cDNA and only primer-probe combinations with an efficiency
385 within 90% and 110% were used. C_q values were obtained with the Bio-Rad CFX Manager 3.1 with
386 C_q Determination Mode set to "Single Threshold" and Baseline Setting set to "Baseline Subtracted
387 Curve Fit". Gene expression was normalized to the geometric mean of the expression values of the

388 reference gene *TFC1* [107]. Statistical significance was assessed with paired two-tailed Student's *t*-
389 test.

390 **Growth Assays**

391 Growth curves were performed automated in a 96 well plate in technical triplicates using the
392 ELx808 Absorbance Microplate Reader (BioTek). Precultures of 100 µl were inoculated at an
393 OD_{600} of 0.1 in round bottom microtiter plates and sealed with an air-permeable membrane
394 (Breathe-Easy; Sigma-Aldrich, St. Louis, MO). The growth curves started at OD_{600} 0.1 and
395 incubated at 30°C for 72 h under constant shaking. The OD_{600} was measured every 10 min.
396 For the Halo assay, strains were grown in liquid YPD media to mid-log phase, washed and plated
397 on YPG plates. A filter plate was placed onto the plate and soaked with 10 µl of a 3 M DTT
398 solution. Plates were incubated at 30°C for 2 days.
399
400 **Preparation of Cell Extracts for Western Blotting**

401 For whole cell lysates yeast strains were cultivated in selective lactate media. Clogger expression
402 was induced by adding 0.5% galactose. After 4.5h, 2 OD_{600}×ml of cells were harvested by
403 centrifugation (5,000g, 5 min, RT) and washed with water. The cells were resuspended in 40
404 µl/OD_{600} 1x Laemmli buffer (125 mM Tris/HCl (pH 6.8), 5% SDS (w/v), 25% glycerol, 0.0005%
405 bromophenol blue) and transferred to a screw-cap tube containing glass beads (0.5 mm). Cell were
406 lysed using a FastPrep-24 5 G homogenizer (MP Biomedicals) with 3 cycles of 20 s, speed 6.0 m/s,
407 120 s breaks, lysis matrix Y. Cell extracts were boiled for 10 min at 96°C. Samples were stored at -
408 20°C until usage. An equal amount of lysate corresponding to 0.4 OD_{600}×ml per sample was loaded
409 on an SDS gel.
410
411 **Immunoblotting**

Proteins were separated by size using discontinuous sodium dodecyl sulfate polyacrylamide gel electrophoresis (SDS-PAGE). They were transferred to a nitrocellulose membrane by semi-dry western blotting with blotting buffer (20 mM Tris, 150 mM glycine, 0.08% SDS (w/v), 20% methanol). To visualize the transferred proteins, the membrane was stained with Ponceau S solution (0.2% (w/v) Ponceau S, 3% (w/v) acetic acid) for 5 min. The membrane was cut in pieces to decorate against several antibodies at once and unspecific binding was blocked by incubation for 30 min in 5% milk in 1X TBS buffer (10 mM Tris/HCl (pH 7.5), 150 mM NaCl). The first antibodies were incubated over night at 4°C. The membrane was washed extensively with 1X TBS Buffer. Afterwards, the membrane was incubated for 90 min at room temperature with the secondary antibody containing the horseradish peroxidase (anti-Rabbit). The membrane was again washed extensively before ECL1 (100 mM Tris/HCl (pH 8.5), 0.044% (w/v) luminol, 0.0066% p-coumaric acid) and ECL2 (100 mM Tris/HCl (pH 8.5), 0.03% H_2O_2) solutions were mixed 1:1 and poured onto the membrane. Thereby chemo luminescence is produced by horseradish peroxidase coupled to the secondary antibody, which was detected on Super RX Medical X-Ray Films (Fuji) using the Optimax Type TR-developer.

Antibodies

The antibodies for the use in immunoblotting of *S. cerevisiae* cell extracts were raised in rabbits using purified recombinant proteins. The secondary antibody was ordered from Biorad (Goat anti-Rabbit IgG (H+L)-HRP Conjugate #172-1019). Antibodies were diluted in 5% (w/v) nonfat dry milk-TBS (Roth T145.2) with the following dilutions: anti-Sod1 1:1,000, anti-Rip1 1:750, anti-Mdj1 1:125, anti-Rabbit 1:10,000. anti-Rip1 and anti-Mdj1 sera were a gift from Thomas Becker.

Split-GFP Assay

Cells containing were transformed with one of the plasmids pYX142-Oxa1-GFP[11], pYX142-Om45-GFP[11], pYX142-Dld1-GFP[11] or pYX142-Mia40-GFP[11] in combination with either pYX122-Sec63-GFP[1-10], pYX122-Oxa1-GFP[1-10], pYX122-Mia40-GFP[1-10] or pYX122-Ssa1-GFP[1-10]. All combinations contained also either the plasmid pYX233-b_2-DHFR or the control plasmid pYX233-cyt DHFR. Cells were grown in selective medium containing 2% lactate to mid log phase. Mitoprotein-induced stress was induced by addition of 0.5% galactose for 4.5 h. 3 OD_{600}×ml were harvested, resuspended in 100 µl medium containing 2% lactate, transferred into a black 96 well plate and centrifuged (5 min at 30 g). The fluorescence was measured with the excitation/emission wavelengths 485±15/530±20 nm in a fluorescence microplate reader (Clariostar, BMG labtech).

For the time course measurement of split-GFP fluorescence in a growing culture, the split-GFP cassette with Oxa1-GFP[11] and Sec63-GFP[1-10] was genomically integrated into the *LEU2* locus of yeast cells. In addition, a constitutively expressed *TEF1p*-ymScarletI was integrated into the *HIS3* locus. The cells were transformed with a pYX233 plasmid for either cytosolic DHFR or b_2-DHFR expression and grown to mid-log phase in synthetic lactate medium. The cells were then diluted to an OD_{600} of 0.4 in 100 µl lactate medium with (inducing) or without (non-inducing) 0.5% galactose in a microtiter plate sealed with an air-permeable membrane (Breathe-Easy; Sigma-Aldrich, St. Louis, MO) in n=6 replicates. A WT strain not expressing no fluorescent protein was used for correction of the background fluorescence of cells or media. The plate was incubated at 30°C under recurrent shaking in a ClarioStar spectrofluorometer (BMG Labtech) and fluorescence was measured every 10 min with the following excitation/emission wavelengths: 485±15/530±20 nm for split-GFP and 580±15/631±36 nm for ymScarletI. Background fluorescence was substracted and the split-GFP signal was divided by the ymScarletI signal to control for growth and overall translation. The average fluorescence intensity at timepoint 0 was set to 1.

Fluorescence microcopy

To analyze the localization of the fluorescence signal in the different split-GFP combinations, mid log phase cultures were shifted to media containing 0,5% galactose to induce the expression of the b_2-DHFR clogger or cytosolic DHFR as control. After centrifugation of 1 OD_{600}×ml of cells (1 min at 16.000 g at RT), the cells were resuspended in 50 µl sterile water. The cell suspension was transferred to a microscope slide for fluorescence imaging using the HCX PL APO 63x oil immersion objective of a Leica TCS SP5II confocal laser scanning microscope. GFP was excited at 488 nm and emission was detected by a photomultiplier through a 530/30-nm band pass filter. Microscopy images were processed using Leica software LAS X (v3.3) and Fiji (v2.1.0).

Ribosome Profiling

Library Preparation

Yeast cultures were grown to mid-log phase in minimal medium containing 2% lactate. Expression of b_2-DHFR or cytosolic DHFR was induced by addition of 0.5% galactose for 4.5 h. Cells were harvested by vacuum filtration (pore size 0.45 µm). In one out of three independent replicates, 100 µg/ml cycloheximide was added to the yeast culture 2 min before harvesting and lysis to inhibit translation elongation, while in the other replicate, cells were not in contact with cycloheximide prior to cell lysis. Cells were flash-frozen in liquid nitrogen and lysed in a mixer mill (Retsch, MM 301) in lysis buffer (20 mM Tris/HCl (pH 7.4), 140 mM KCl, 1.5 mM $MgCl_2$, 0.5 mM DTT, 100 µg/ml cycloheximide, 1% (v/v) Triton X-100) in 50 ml stainless steel grinding chambers under cryogenic conditions for 1 min at 20 Hz. Lysates were thawed in a water bath at room temperature, immediately followed by centrifugation at 15,000 g at 4°C for 10 min. RNA concentration was quantified with a NanoDrop fluorometer (absorbance at 260 nm) and RNA digestion was performed with RNase I (Ambion, #AM2294, 2.5 µl / mg RNA) for 45 min at room temperature. Digestion was stopped by the addition of SUPERase·In RNase inhibitor (Ambion, #AM2696, 2 µl / 100 µl digestion). Ribosomes were isolate by centrifugation through a 25% (w/v) sucrose cushion in a

TLA 100.2 rotor (Beckman) at 72,000 rpm for 20 min at 4°C. RNA was extracted from the ribosomal pellet using the hot SDS-Phenol-Chloroform method and 24-35 nt ribosome footprints were size selected on a 15% (w/v) polyacrylamide TBE-urea gel. Ribosomal RNA was removed with the RiboZero Gold kit (Illumina). Sequencing libraries were then prepared as previously described [108]. Libraries were quantified by qPCR (Kapa Biosystems) and sequenced using a HiSeq 4000 (Illumina).

Data analysis

Sequencing reads were demultiplexed with Illumina CASAVA v1.8 and adaptor sequences were trimmed using Cutadapt v2.8. Reads that mapped to ribosomal RNAs were removed using Bowtie v.1.2.3 [109] and remaining reads were aligned to the yeast reference genome obtained from the *Saccharomyces* genome database (genome release R64-2-1).

For each read, reads were summed at each nucleotide by customized python scripts. Metagene analysis was performed separately on each fragment length to remove lengths that did not exhibit the 3-nucleotide periodicity that is characteristic for ribosome footprints. Each of the remaining reads was assigned to the first A-site nucleotide. To this end, a nucleotide offset from the 5' end of each fragment length was empirically determined, using the characteristic high ribosome density at the start codon. Nucleotide reads at each codon were then summed and used for all downstream analysis.

Gene-level differential expression analysis was performed using HTSeq [110] and the DESeq2 package [111] within the Bioconductor v3.12 project in the statistical programming language R v.4.0.3 [112].

Analysis of published datasets on mRNA localization

The dataset on translation close to the ER and mitochondrial surface in yeast was obtained from Jan et al. (2014)[59]. In this study, the authors fused the biotin ligase BirA to Sec63 (ER) or Om45

(mitochondrial) and pulled down ribosomes that were biotinylated after a short pulse of biotin and translation inhibition with cycloheximide (CHX). The genes were filtered for those that code for mitochondrial proteins according to [70] and $\log_2$ fold enrichments of ribosome footprints at the ER (7 min CHX) or mitochondrial membranes (2 min CHX) over total ribosome footprints were plotted.

The dataset on transcript localization in human cells was obtained from Fazal et al. (2019)[61]. Here, the authors used the biotin ligase APEX2 fused to proteins of different cellular localizations to directly biotinylate RNA. Mitochondrial genes were filtered according to MitoCarta 3.0 [113] and $\log_2$ fold enrichment of ER- or mitochondria-localized transcripts over total transcripts were plotted.

The dataset on the SRP-bound translatome in yeast was obtained from Chartron et al. (2016)[63]. The authors compared ribosome-nascent chain complexes purified by pulldown of SRP to total ribosomes by ribosome profiling. Genes coding for secretory, cytosolic and mitochondrial proteins were filtered according to the author's categorization and the distribution of the $\log_2$ fold enrichment of SRP-bound polysomes over total ribosome footprints was plotted.

Data and material availability

The data produced in this study are presented in this published article and its supplementary material. The ribosome profiling data on clogger-expressing yeast cells are deposited into GEO [114] with accession number GSE172017.

All yeast strains, plasmids and primers used in this study are listed in Supplementary Tables 1-3 and are available from the authors upon request. The plasmids pYX233 DHFR and pYX233 b_2-DHFR for expression of the mitochondrial clogger are available via Addgene (plasmids #163761 and #163759).

Author contributions

F.B. and J.F. conceived and supervised the study. F.B. and K.C.S. prepared the ribosome profiling libraries and performed the bioinformatics analysis of the sequencing data. K.K., L.K., C.G. and F.B. generated constructs and strains. K.K., L.K. and C.G. performed *in vivo* experiments. K.K. and F.B. analyzed *HAC1* splicing by RT-PCR. K.K. established and performed the split-GFP assay. K.K. performed fluorescence microscopy and K.K. and K.G.H. analyzed the results. K.G.H. and F.B. analyzed ribosome profiling data on localized and SRP-bound translation of mitochondrial proteins. K.K., C.G., L.K., K.G.H., J.M.H., J.F. and F.B. analyzed the data. F.B. wrote the manuscript with input from all authors.

Acknowledgements

Sequencing was performed at the UCSF Center for Advanced Technology. We thank Sabine Knaus, Andrea Trinkaus and Natalia M. Barbosa for assistance with the experiments and Torsten Möhlmann for help with the microscopy. We thank T. Kelly Rainbolt and Sebastian Schuck for discussions and comments on the manuscript. This project was funded by grants from the Landesforschungsinitiative Rheinland-Pfalz BioComp (to F.B. and J.M.H.), the Deutsche Forschungsgemeinschaft (DE2803/10 to J.M.H.), the US National Institutes of Health (NIH GM56433 to J.F. and AG047126 to K.C.S.), the Glenn Foundation for Medical Research (Postdoctoral Fellowship to K.C.S.), the Company of Biologists (Travelling Fellowship JCSTF181148 to F.B.), the European Molecular Biology Organization (Long-Term Fellowship ALT 762-2019 to K.G.H.), the Helen Hay Whitney Foundation (F-1240 to K.G.H.) and the Joachim Herz Stiftung (to F.B. and C.G.).

Competing interests

The authors declare that they have no competing interests.

559

References

1 Klaips, C. L., Jayaraj, G. G. & Hartl, F. U. Pathways of cellular proteostasis in aging and disease. *J Cell Biol* **217**, 51-63, doi:10.1083/jcb.201709072 (2018).

2 Hipp, M. S., Park, S. H. & Hartl, F. U. Proteostasis impairment in protein-misfolding and -aggregation diseases. *Trends Cell Biol* **24**, 506-514, doi:10.1016/j.tcb.2014.05.003 (2014).

3 Gidalevitz, T., Ben-Zvi, A., Ho, K. H., Brignull, H. R. & Morimoto, R. I. Progressive disruption of cellular protein folding in models of polyglutamine diseases. *Science* **311**, 1471-1474, doi:10.1126/science.1124514 (2006).

4 Moehle, E. A., Shen, K. & Dillin, A. Mitochondrial proteostasis in the context of cellular and organismal health and aging. *J Biol Chem* **294**, 5396-5407, doi:10.1074/jbc.TM117.000893 (2019).

5 Aviner, R. & Frydman, J. Proteostasis in Viral Infection: Unfolding the Complex Virus-Chaperone Interplay. *Cold Spring Harb Perspect Biol* **12**, doi:10.1101/cshperspect.a034090 (2020).

6 Naresh, N. U. & Haynes, C. M. Signaling and Regulation of the Mitochondrial Unfolded Protein Response. *Cold Spring Harb Perspect Biol* **11**, a033944, doi:10.1101/cshperspect.a033944 (2019).

7 Karagöz, G. E., Acosta-Alvear, D. & Walter, P. The Unfolded Protein Response: Detecting and Responding to Fluctuations in the Protein-Folding Capacity of the Endoplasmic Reticulum. *Cold Spring Harb Perspect Biol* **11**, a033886, doi:10.1101/cshperspect.a033886 (2019).

8 Pincus, D. Regulation of Hsf1 and the Heat Shock Response. *Adv Exp Med Biol* **1243**, 41-50, doi:10.1007/978-3-030-40204-4_3 (2020).

9 Münch, C. The different axes of the mammalian mitochondrial unfolded protein response. *BMC Biol* **16**, 81, doi:10.1186/s12915-018-0548-x (2018).

10 Cox, J. S. & Walter, P. A novel mechanism for regulating activity of a transcription factor that controls the unfolded protein response. *Cell* **87**, 391-404, doi:10.1016/s0092-8674(00)81360-4 (1996).

11 Walter, P. & Ron, D. The unfolded protein response: from stress pathway to homeostatic regulation. *Science* **334**, 1081-1086, doi:10.1126/science.1209038 (2011).

12 Kornmann, B. *et al.* An ER-mitochondria tethering complex revealed by a synthetic biology screen. *Science* **325**, 477-481, doi:10.1126/science.1175088 (2009).

13 Valm, A. M. *et al.* Applying systems-level spectral imaging and analysis to reveal the organelle interactome. *Nature* **546**, 162-167, doi:10.1038/nature22369 (2017).

14 Bohnert, M. Tether Me, Tether Me Not-Dynamic Organelle Contact Sites in Metabolic Rewiring. *Dev Cell* **54**, 212-225, doi:10.1016/j.devcel.2020.06.026 (2020).

15 Hansen, K. G. *et al.* An ER surface retrieval pathway safeguards the import of mitochondrial membrane proteins in yeast. *Science* **361**, 1118-1122, doi:10.1126/science.aar8174 (2018).

16 Carreras-Sureda, A. *et al.* Non-canonical function of IRE1alpha determines mitochondria-associated endoplasmic reticulum composition to control calcium transfer and bioenergetics. *Nat Cell Biol* **21**, 755-767, doi:10.1038/s41556-019-0329-y (2019).

17 Bauerlein, F. J. B. *et al.* In Situ Architecture and Cellular Interactions of PolyQ Inclusions. *Cell* **171**, 179-187 e110, doi:10.1016/j.cell.2017.08.009 (2017).

18 Hetz, C. & Mollereau, B. Disturbance of endoplasmic reticulum proteostasis in neurodegenerative diseases. *Nat Rev Neurosci* **15**, 233-249, doi:10.1038/nrn3689 (2014).

19 Boos, F., Labbadia, J. & Herrmann, J. M. How the Mitoprotein-Induced Stress Response Safeguards the Cytosol: A Unified View. *Trends Cell Biol* **30**, 241-254, doi:10.1016/j.tcb.2019.12.003 (2020).

20 Liu, Y. & Chang, A. Heat shock response relieves ER stress. *EMBO J* **27**, 1049-1059, doi:10.1038/emboj.2008.42 (2008).

21 Schmidt, R. M., Schessner, J. P., Borner, G. H. & Schuck, S. The proteasome biogenesis regulator Rpn4 cooperates with the unfolded protein response to promote ER stress resistance. *Elife* **8**, e43244, doi:10.7554/eLife.43244 (2019).

22 Lebeau, J. *et al.* The PERK Arm of the Unfolded Protein Response Regulates Mitochondrial Morphology during Acute Endoplasmic Reticulum Stress. *Cell Rep* **22**, 2827-2836, doi:10.1016/j.celrep.2018.02.055 (2018).

23 Pincus, D., Aranda-Diaz, A., Zuleta, I. A., Walter, P. & El-Samad, H. Delayed Ras/PKA signaling augments the unfolded protein response. *Proc Natl Acad Sci U S A* **111**, 14800-14805, doi:10.1073/pnas.1409588111 (2014).

24 Rolland, S. G. *et al.* Compromised Mitochondrial Protein Import Acts as a Signal for UPR(mt). *Cell Rep* **28**, 1659-1669 e1655, doi:10.1016/j.celrep.2019.07.049 (2019).

25 Nargund, A. M., Pellegrino, M. W., Fiorese, C. J., Baker, B. M. & Haynes, C. M. Mitochondrial import efficiency of ATFS-1 regulates mitochondrial UPR activation. *Science* **337**, 587-590, doi:10.1126/science.1223560 (2012).

26 Harbauer, A. B., Zahedi, R. P., Sickmann, A., Pfanner, N. & Meisinger, C. The protein import machinery of mitochondria-a regulatory hub in metabolism, stress, and disease. *Cell Metab* **19**, 357-372, doi:10.1016/j.cmet.2014.01.010 (2014).

27 Wrobel, L. *et al.* Mistargeted mitochondrial proteins activate a proteostatic response in the cytosol. *Nature* **524**, 485-488, doi:10.1038/nature14951 (2015).

28 Boos, F. *et al.* Mitochondrial protein-induced stress triggers a global adaptive transcriptional programme. *Nat Cell Biol* **21**, 442-451, doi:10.1038/s41556-019-0294-5 (2019).

29 Kim, H. E. *et al.* Lipid Biosynthesis Coordinates a Mitochondrial-to-Cytosolic Stress Response. *Cell* **166**, 1539-1552 e1516, doi:10.1016/j.cell.2016.08.027 (2016).

30 Nargund, A. M., Fiorese, C. J., Pellegrino, M. W., Deng, P. & Haynes, C. M. Mitochondrial and nuclear accumulation of the transcription factor ATFS-1 promotes OXPHOS recovery during the UPR(mt). *Mol Cell* **58**, 123-133, doi:10.1016/j.molcel.2015.02.008 (2015).

31 Wang, X. & Chen, X. J. A cytosolic network suppressing mitochondria-mediated proteostatic stress and cell death. *Nature* **524**, 481-484, doi:10.1038/nature14859 (2015).

32 Fiorese, C. J. *et al.* The Transcription Factor ATF5 Mediates a Mammalian Mitochondrial UPR. *Curr Biol* **26**, 2037-2043, doi:10.1016/j.cub.2016.06.002 (2016).

33 Labbadia, J. *et al.* Mitochondrial Stress Restores the Heat Shock Response and Prevents Proteostasis Collapse during Aging. *Cell Rep* **21**, 1481-1494, doi:10.1016/j.celrep.2017.10.038 (2017).

34 Guo, X. *et al.* Mitochondrial stress is relayed to the cytosol by an OMA1-DELE1-HRI pathway. *Nature* **579**, 427-432, doi:10.1038/s41586-020-2078-2 (2020).

35 Weidberg, H. & Amon, A. MitoCPR-A surveillance pathway that protects mitochondria in response to protein import stress. *Science* **360**, eaan4146, doi:10.1126/science.aan4146 (2018).

36 Mårtensson, C. U. *et al.* Mitochondrial protein translocation-associated degradation. *Nature* **569**, 679-683, doi:10.1038/s41586-019-1227-y (2019).

37 Wienhues, U. *et al.* Protein folding causes an arrest of preprotein translocation into mitochondria in vivo. *J Cell Biol* **115**, 1601-1609, doi:10.1083/jcb.115.6.1601 (1991).

38 Rassow, J. *et al.* Translocation arrest by reversible folding of a precursor protein imported into mitochondria. A means to quantitate translocation contact sites. *J Cell Biol* **109**, 1421-1428, doi:10.1083/jcb.109.4.1421 (1989).

39 Eilers, M. & Schatz, G. Binding of a specific ligand inhibits import of a purified precursor protein into mitochondria. *Nature* **322**, 228-232, doi:10.1038/322228a0 (1986).

40 Samluk, L. *et al.* Cytosolic translational responses differ under conditions of severe short-term and long-term mitochondrial stress. *Mol Biol Cell* **30**, 1864-1877, doi:10.1091/mbc.E18-10-0628 (2019).

41 Tsaytler, P., Harding, H. P., Ron, D. & Bertolotti, A. Selective inhibition of a regulatory subunit of protein phosphatase 1 restores proteostasis. *Science* **332**, 91-94, doi:10.1126/science.1201396 (2011).

42 Morimoto, R. I. Heat shock: the role of transient inducible responses in cell damage, transformation, and differentiation. *Cancer Cells* **3**, 295-301 (1991).

43 Mesecke, N. *et al.* A disulfide relay system in the intermembrane space of mitochondria that mediates protein import. *Cell* **121**, 1059-1069, doi:10.1016/j.cell.2005.04.011 (2005).

44 Chacinska, A. *et al.* Essential role of Mia40 in import and assembly of mitochondrial intermembrane space proteins. *EMBO J* **23**, 3735-3746, doi:10.1038/sj.emboj.7600389 (2004).

45 Weill, U. *et al.* Assessment of GFP Tag Position on Protein Localization and Growth Fitness in Yeast. *J Mol Biol* **431**, 636-641, doi:10.1016/j.jmb.2018.12.004 (2019).

46 Wigley, W. C., Stidham, R. D., Smith, N. M., Hunt, J. F. & Thomas, P. J. Protein solubility and folding monitored in vivo by structural complementation of a genetic marker protein. *Nat Biotechnol* **19**, 131-136, doi:10.1038/84389 (2001).

47 Waldo, G. S., Standish, B. M., Berendzen, J. & Terwilliger, T. C. Rapid protein-folding assay using green fluorescent protein. *Nat Biotechnol* **17**, 691-695, doi:10.1038/10904 (1999).

48 Smoyer, C. J. *et al.* Analysis of membrane proteins localizing to the inner nuclear envelope in living cells. *J Cell Biol* **215**, 575-590, doi:10.1083/jcb.201607043 (2016).

49 Cabantous, S. & Waldo, G. S. In vivo and in vitro protein solubility assays using split GFP. *Nat Methods* **3**, 845-854, doi:10.1038/nmeth932 (2006).

50 Cabantous, S., Terwilliger, T. C. & Waldo, G. S. Protein tagging and detection with engineered self-assembling fragments of green fluorescent protein. *Nat Biotechnol* **23**, 102-107, doi:10.1038/nbt1044 (2005).

51 Pedelacq, J. D., Cabantous, S., Tran, T., Terwilliger, T. C. & Waldo, G. S. Engineering and characterization of a superfolder green fluorescent protein. *Nat Biotechnol* **24**, 79-88, doi:10.1038/nbt1172 (2006).

52 Wenz, L. S. *et al.* The presequence pathway is involved in protein sorting to the mitochondrial outer membrane. *EMBO Rep* **15**, 678-685, doi:10.1002/embr.201338144 (2014).

53 Song, J., Tamura, Y., Yoshihisa, T. & Endo, T. A novel import route for an N-anchor mitochondrial outer membrane protein aided by the TIM23 complex. *EMBO Rep* **15**, 670-677, doi:10.1002/embr.201338142 (2014).

54 Szyrach, G., Ott, M., Bonnefoy, N., Neupert, W. & Herrmann, J. M. Ribosome binding to the Oxa1 complex facilitates co-translational protein insertion in mitochondria. *EMBO J* **22**, 6448-6457, doi:10.1093/emboj/cdg623 (2003).

55 Terziyska, N. *et al.* Mia40, a novel factor for protein import into the intermembrane space of mitochondria is able to bind metal ions. *FEBS Lett* **579**, 179-184, doi:10.1016/j.febslet.2004.11.072 (2005).

56 Kater, L. *et al.* Structure of the Bcs1 AAA-ATPase suggests an airlock-like translocation mechanism for folded proteins. *Nat Struct Mol Biol* **27**, 142-149, doi:10.1038/s41594-019-0364-1 (2020).

57 Rojo, E. E., Guiard, B., Neupert, W. & Stuart, R. A. Sorting of D-lactate dehydrogenase to the inner membrane of mitochondria. Analysis of topogenic signal and energetic requirements. *J Biol Chem* **273**, 8040-8047, doi:10.1074/jbc.273.14.8040 (1998).

58 Wu, X., Cabanos, C. & Rapoport, T. A. Structure of the post-translational protein translocation machinery of the ER membrane. *Nature* **566**, 136-139, doi:10.1038/s41586-018-0856-x (2019).

59 Jan, C. H., Williams, C. C. & Weissman, J. S. Principles of ER cotranslational translocation revealed by proximity-specific ribosome profiling. *Science* **346**, 1257521, doi:10.1126/science.1257521 (2014).

60 Williams, C. C., Jan, C. H. & Weissman, J. S. Targeting and plasticity of mitochondrial proteins revealed by proximity-specific ribosome profiling. *Science* **346**, 748-751, doi:10.1126/science.1257522 (2014).

61 Fazal, F. M. *et al.* Atlas of Subcellular RNA Localization Revealed by APEX-Seq. *Cell* **178**, 473-490 e426, doi:10.1016/j.cell.2019.05.027 (2019).

62 del Alamo, M. *et al.* Defining the specificity of cotranslationally acting chaperones by systematic analysis of mRNAs associated with ribosome-nascent chain complexes. *PLoS Biol* **9**, e1001100, doi:10.1371/journal.pbio.1001100 (2011).

63 Chartron, J. W., Hunt, K. C. & Frydman, J. Cotranslational signal-independent SRP preloading during membrane targeting. *Nature* **536**, 224-228, doi:10.1038/nature19309 (2016).

64 Ng, D. T., Brown, J. D. & Walter, P. Signal sequences specify the targeting route to the endoplasmic reticulum membrane. *J Cell Biol* **134**, 269-278, doi:10.1083/jcb.134.2.269 (1996).

65 Walter, P. & Blobel, G. Translocation of proteins across the endoplasmic reticulum III. Signal recognition protein (SRP) causes signal sequence-dependent and site-specific arrest of chain elongation that is released by microsomal membranes. *J Cell Biol* **91**, 557-561, doi:10.1083/jcb.91.2.557 (1981).

66 Costa, E. A., Subramanian, K., Nunnari, J. & Weissman, J. S. Defining the physiological role of SRP in protein-targeting efficiency and specificity. *Science* **359**, 689-692, doi:10.1126/science.aar3607 (2018).

67 Wild, K., Halic, M., Sinning, I. & Beckmann, R. SRP meets the ribosome. *Nat Struct Mol Biol* **11**, 1049-1053, doi:10.1038/nsmb853 (2004).

68 Paulo, J. A. *et al.* Quantitative mass spectrometry-based multiplexing compares the abundance of 5000 S. cerevisiae proteins across 10 carbon sources. *J Proteomics* **148**, 85-93, doi:10.1016/j.jprot.2016.07.005 (2016).

69 Paulo, J. A., O'Connell, J. D., Gaun, A. & Gygi, S. P. Proteome-wide quantitative multiplexed profiling of protein expression: carbon-source dependency in Saccharomyces cerevisiae. *Mol Biol Cell* **26**, 4063-4074, doi:10.1091/mbc.E15-07-0499 (2015).

70 Morgenstern, M. *et al.* Definition of a High-Confidence Mitochondrial Proteome at Quantitative Scale. *Cell Rep* **19**, 2836-2852, doi:10.1016/j.celrep.2017.06.014 (2017).

71 Di Bartolomeo, F. *et al.* Absolute yeast mitochondrial proteome quantification reveals trade-off between biosynthesis and energy generation during diauxic shift. *Proc Natl Acad Sci U S A* **117**, 7524-7535, doi:10.1073/pnas.1918216117 (2020).

72 Murphy, J. P., Stepanova, E., Everley, R. A., Paulo, J. A. & Gygi, S. P. Comprehensive Temporal Protein Dynamics during the Diauxic Shift in Saccharomyces cerevisiae. *Mol Cell Proteomics* **14**, 2454-2465, doi:10.1074/mcp.M114.045849 (2015).

73 Rubio, C. *et al.* Homeostatic adaptation to endoplasmic reticulum stress depends on Ire1 kinase activity. *J Cell Biol* **193**, 171-184, doi:10.1083/jcb.201007077 (2011).

74 Chawla, A., Chakrabarti, S., Ghosh, G. & Niwa, M. Attenuation of yeast UPR is essential for survival and is mediated by IRE1 kinase. *J Cell Biol* **193**, 41-50, doi:10.1083/jcb.201008071 (2011).

75 Shakya, V. P. *et al.* A nuclear-based quality control pathway for non-imported mitochondrial proteins. *Elife* **10**, doi:10.7554/eLife.61230 (2021).

76 Kowalski, L. *et al.* Determinants of the cytosolic turnover of mitochondrial intermembrane space proteins. *BMC Biol* **16**, 66, doi:10.1186/s12915-018-0536-1 (2018).

77 Nowicka, U. *et al.* Cytosolic aggregation of mitochondrial proteins disrupts cellular homeostasis by stimulating other proteins aggregation. *bioRxiv*, 2021.2005.2002.442342, doi:10.1101/2021.05.02.442342 (2021).

78 Liu, Y. *et al.* Mitochondrial carrier protein overloading and misfolding induce aggresomes and proteostatic adaptations in the cytosol. *Mol Biol Cell* **30**, 1272-1284, doi:10.1091/mbc.E19-01-0046 (2019).

79 Backes, S. *et al.* The chaperone-binding activity of the mitochondrial surface receptor Tom70 protects the cytosol against mitoprotein-induced stress. *Cell Rep* **35**, 108936, doi:10.1016/j.celrep.2021.108936 (2021).

80 Vincenz-Donnelly, L. *et al.* High capacity of the endoplasmic reticulum to prevent secretion and aggregation of amyloidogenic proteins. *EMBO J* **37**, 337-350, doi:10.15252/embj.201695841 (2018).

81 Rousseau, E. *et al.* Targeting expression of expanded polyglutamine proteins to the endoplasmic reticulum or mitochondria prevents their aggregation. *Proc Natl Acad Sci U S A* **101**, 9648-9653, doi:10.1073/pnas.0403015101 (2004).

82 Metzger, M. B., Maurer, M. J., Dancy, B. M. & Michaelis, S. Degradation of a cytosolic protein requires endoplasmic reticulum-associated degradation machinery. *J Biol Chem* **283**, 32302-32316, doi:10.1074/jbc.M806424200 (2008).

83 Laborenz, J. *et al.* The ER protein Ema19 facilitates the degradation of non-imported mitochondrial precursor proteins. *Mol Biol Cell*, mbcE20110748, doi:10.1091/mbc.E20-11-0748 (2021).

84 Tran, J. R., Tomsic, L. R. & Brodsky, J. L. A Cdc48p-associated factor modulates endoplasmic reticulum-associated degradation, cell stress, and ubiquitinated protein homeostasis. *J Biol Chem* **286**, 5744-5755, doi:10.1074/jbc.M110.179259 (2011).

85 Heo, J. M. *et al.* A stress-responsive system for mitochondrial protein degradation. *Mol Cell* **40**, 465-480, doi:10.1016/j.molcel.2010.10.021 (2010).

86 Caplan, A. J., Cyr, D. M. & Douglas, M. G. YDJ1p facilitates polypeptide translocation across different intracellular membranes by a conserved mechanism. *Cell* **71**, 1143-1155, doi:10.1016/s0092-8674(05)80063-7 (1992).

87 Opaliński, Ł. *et al.* Recruitment of Cytosolic J-Proteins by TOM Receptors Promotes Mitochondrial Protein Biogenesis. *Cell Rep* **25**, 2036-2043 e2035, doi:10.1016/j.celrep.2018.10.083 (2018).

88 Xiao, T., Shakya, V. P. & Hughes, A. L. ER targeting of non-imported mitochondrial carrier proteins is dependent on the GET pathway. *Life Sci Alliance* **4**, doi:10.26508/lsa.202000918 (2021).

89 Matsumoto, S. *et al.* Msp1 Clears Mistargeted Proteins by Facilitating Their Transfer from Mitochondria to the ER. *Mol Cell* **76**, 191-205 e110, doi:10.1016/j.molcel.2019.07.006 (2019).

90 Dederer, V. *et al.* Cooperation of mitochondrial and ER factors in quality control of tail-anchored proteins. *Elife* **8**, doi:10.7554/eLife.45506 (2019).

91 McKenna, M. J. *et al.* The endoplasmic reticulum P5A-ATPase is a transmembrane helix dislocase. *Science* **369**, doi:10.1126/science.abc5809 (2020).

92 Hayashi, T., Rizzuto, R., Hajnoczky, G. & Su, T. P. MAM: more than just a housekeeper. *Trends Cell Biol* **19**, 81-88, doi:10.1016/j.tcb.2008.12.002 (2009).

93 Munoz, J. P. *et al.* Mfn2 modulates the UPR and mitochondrial function via repression of PERK. *EMBO J* **32**, 2348-2361, doi:10.1038/emboj.2013.168 (2013).

94 Böckler, S. & Westermann, B. Mitochondrial ER contacts are crucial for mitophagy in yeast. *Dev Cell* **28**, 450-458, doi:10.1016/j.devcel.2014.01.012 (2014).

95 Hamasaki, M. *et al.* Autophagosomes form at ER-mitochondria contact sites. *Nature* **495**, 389-393, doi:10.1038/nature11910 (2013).

96 Vitali, D. G. *et al.* The GET pathway can increase the risk of mitochondrial outer membrane proteins to be mistargeted to the ER. *J Cell Sci* **131**, doi:10.1242/jcs.211110 (2018).

97 Rainbolt, T. K., Saunders, J. M. & Wiseman, R. L. Stress-responsive regulation of mitochondria through the ER unfolded protein response. *Trends Endocrinol Metab* **25**, 528-537, doi:10.1016/j.tem.2014.06.007 (2014).

98 Eiyama, A., Aaltonen, M. J., Nolte, H., Tatsuta, T. & Langer, T. Disturbed intramitochondrial phosphatidic acid transport impairs cellular stress signaling. *J Biol Chem*, 100335, doi:10.1016/j.jbc.2021.100335 (2021).

99 Tran, D. M., Ishiwata-Kimata, Y., Mai, T. C., Kubo, M. & Kimata, Y. The unfolded protein response alongside the diauxic shift of yeast cells and its involvement in mitochondria enlargement. *Sci Rep* **9**, 12780, doi:10.1038/s41598-019-49146-5 (2019).

100 Yong, J. *et al.* Mitochondria supply ATP to the ER through a mechanism antagonized by cytosolic Ca(2). *Elife* **8**, doi:10.7554/eLife.49682 (2019).

101 Costa, R. *et al.* Impaired Mitochondrial ATP Production Downregulates Wnt Signaling via ER Stress Induction. *Cell Rep* **28**, 1949-1960 e1946, doi:10.1016/j.celrep.2019.07.050 (2019).

102 Balsa, E. *et al.* ER and Nutrient Stress Promote Assembly of Respiratory Chain Supercomplexes through the PERK-eIF2alpha Axis. *Mol Cell* **74**, 877-890 e876, doi:10.1016/j.molcel.2019.03.031 (2019).

103 Sikorski, R. S. & Hieter, P. A system of shuttle vectors and yeast host strains designed for efficient manipulation of DNA in Saccharomyces cerevisiae. *Genetics* **122**, 19-27 (1989).

104 Thomas, B. J. & Rothstein, R. Elevated recombination rates in transcriptionally active DNA. *Cell* **56**, 619-630, doi:10.1016/0092-8674(89)90584-9 (1989).

105 Botman, D., de Groot, D. H., Schmidt, P., Goedhart, J. & Teusink, B. In vivo characterisation of fluorescent proteins in budding yeast. *Sci Rep* **9**, 2234, doi:10.1038/s41598-019-38913-z (2019).

106 Janke, C. *et al.* A versatile toolbox for PCR-based tagging of yeast genes: new fluorescent proteins, more markers and promoter substitution cassettes. *Yeast* **21**, 947-962, doi:10.1002/yea.1142 (2004).

107 Livak, K. J. & Schmittgen, T. D. Analysis of relative gene expression data using real-time quantitative PCR and the 2(-Delta Delta C(T)) Method. *Methods* **25**, 402-408, doi:10.1006/meth.2001.1262 (2001).

108 Ingolia, N. T., Brar, G. A., Rouskin, S., McGeachy, A. M. & Weissman, J. S. The ribosome profiling strategy for monitoring translation in vivo by deep sequencing of ribosome-protected mRNA fragments. *Nat Protoc* **7**, 1534-1550, doi:10.1038/nprot.2012.086 (2012).

109 Langmead, B., Trapnell, C., Pop, M. & Salzberg, S. L. Ultrafast and memory-efficient alignment of short DNA sequences to the human genome. *Genome Biol* **10**, R25, doi:10.1186/gb-2009-10-3-r25 (2009).

110 Anders, S., Pyl, P. T. & Huber, W. HTSeq--a Python framework to work with high-throughput sequencing data. *Bioinformatics* **31**, 166-169, doi:10.1093/bioinformatics/btu638 (2015).

111 Love, M. I., Huber, W. & Anders, S. Moderated estimation of fold change and dispersion for RNA-seq data with DESeq2. *Genome Biol* **15**, 550, doi:10.1186/s13059-014-0550-8 (2014).

112 Huber, W. *et al.* Orchestrating high-throughput genomic analysis with Bioconductor. *Nat Methods* **12**, 115-121, doi:10.1038/nmeth.3252 (2015).

113 Rath, S. *et al.* MitoCarta3.0: an updated mitochondrial proteome now with sub-organelle localization and pathway annotations. *Nucleic Acids Res* **49**, D1541-D1547, doi:10.1093/nar/gkaa1011 (2021).

114 Barrett, T. *et al.* NCBI GEO: archive for functional genomics data sets--update. *Nucleic Acids Res* **41**, D991-995, doi:10.1093/nar/gks1193 (2013).

Figures and Figure Legends

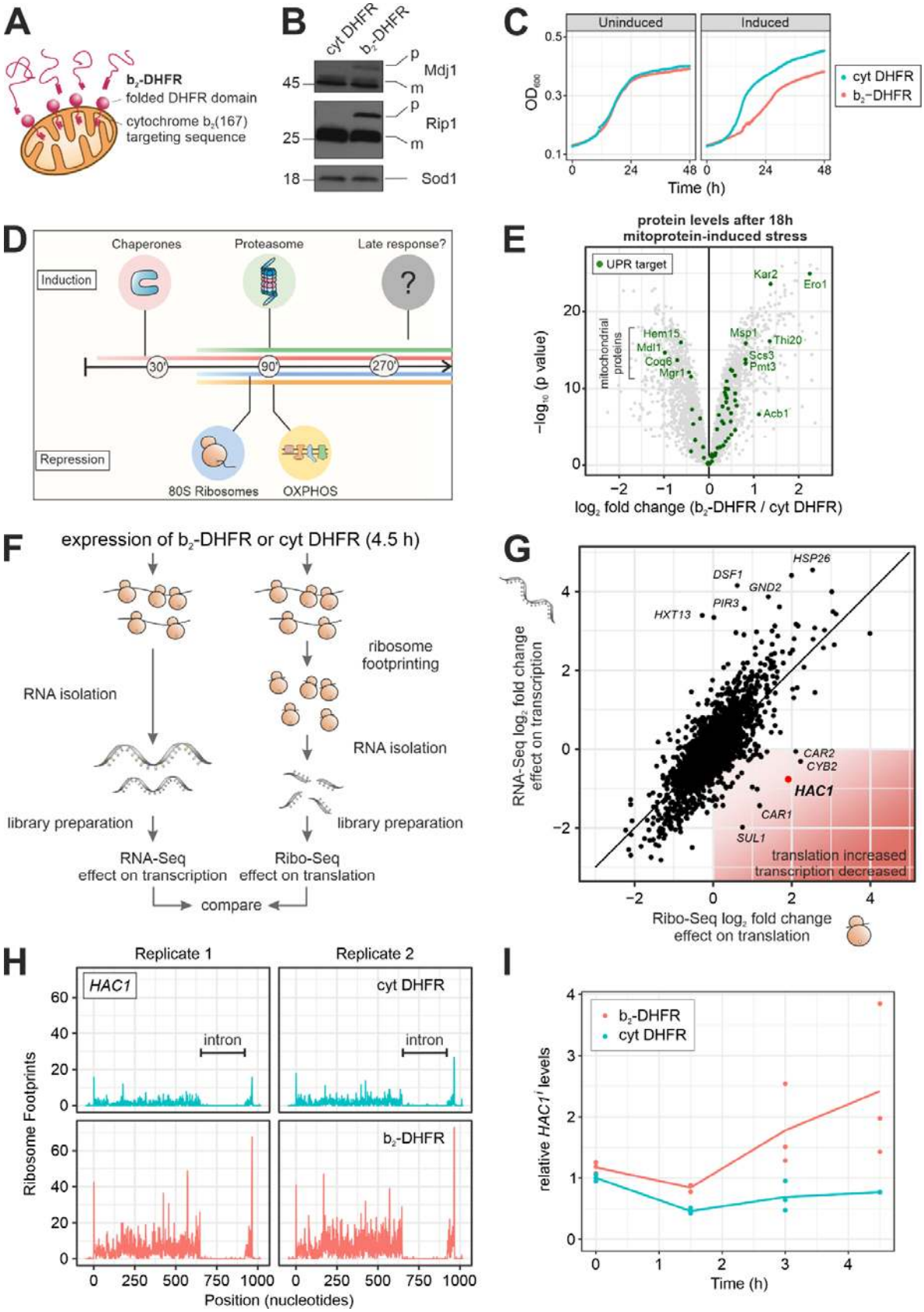

837 **Figure 1. Mitoprotein-induced stress triggers the UPR^{ER}. A,** Fusion of DHFR to the N-terminus
838 of Cytochrome b_2 generates a mitochondrial 'clogger' that jams the protein import machinery. **B,**
839 The mitochondrial clogger b_2-DHFR or cytosolic DHFR were expressed for 4.5 h. The precursor
840 form of the mitochondrial proteins Mdj1 and Rip1 were detected by Western Blotting. **C,**
841 Expression of b_2-DHFR leads to attenuated growth. **D,** The mitoprotein-induced stress response
842 encompasses an early transcriptional induction of chaperones and the proteasome and a
843 downregulation of cytosolic ribosomes and OXPHOS components. **E,** Protein levels in clogger-
844 expressing versus control cells after 18 h of induction were measured by quantitative mass
845 spectrometry [28]. Highlighted are proteins which are reported targets of the UPR^{ER} [21]. Data from n=3
846 independent biological replicates are shown. **F, G,** The cellular transcriptome and translatome after
847 4.5 h of clogger induction were measured by RNA-Seq (n=4) [28] and ribosome profiling (n=3),
848 respectively. Shown are $\log_2$ fold changes of b_2-DHFR versus cytosolic DHFR. *HAC1* transcripts
849 are slightly reduced, but its translation is upregulated. **H,** Ribosome footprints along the *HAC1* gene
850 from cells expressing b_2-DHFR or cytosolic DHFR for 4.5 h are shown. **I,** Levels of spliced *HAC1*
851 mRNA in cells expressing b_2-DHFR or cytosolic DHFR were measured by RT-qPCR over time
852 (n=3).

853

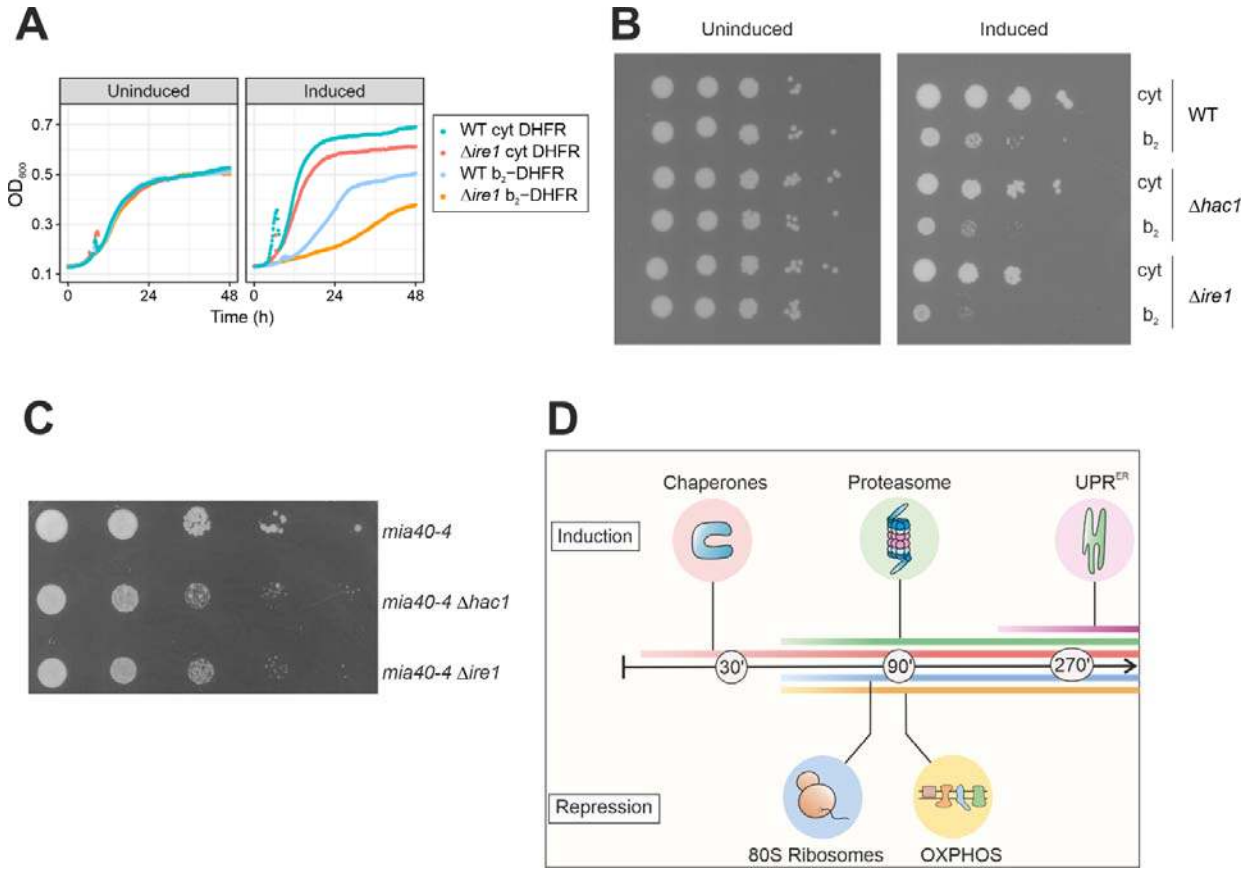

Figure 2. The UPR^{ER} is required for cellular fitness under mitoprotein-induced stress conditions. A, Wild type and Δ*ire1* cells were grown under non-inducing (left) or inducing (right) conditions, expressing either b_2-DHFR or cytosolic DHFR. Δ*ire1* cells are more susceptible to mitoprotein-induced stress. **B,** Tenfold serial dilutions of wild type, Δ*ire1* and Δ*hac1* cultures were dropped on lactate plates with ('induced) or without ('uninduced') 0.5% galactose. The UPR^{ER}-deficient mutants show synthetic growth defects with expression of b_2-DHFR. **C,** *HAC1* and *IRE1* were deleted in temperature-sensitive *mia40-4* mutants. Cells were grown in glucose medium and serial dilutions were spotted on glucose plates and incubated at the semi-permissive temperature of 30°C. Loss of the UPR^{ER} results in synthetic growth defects. **D,** Early cytonuclear adaptations to mitoprotein-induced stress are accompanied by the induction of the UPR^{ER} as a second line of defense.

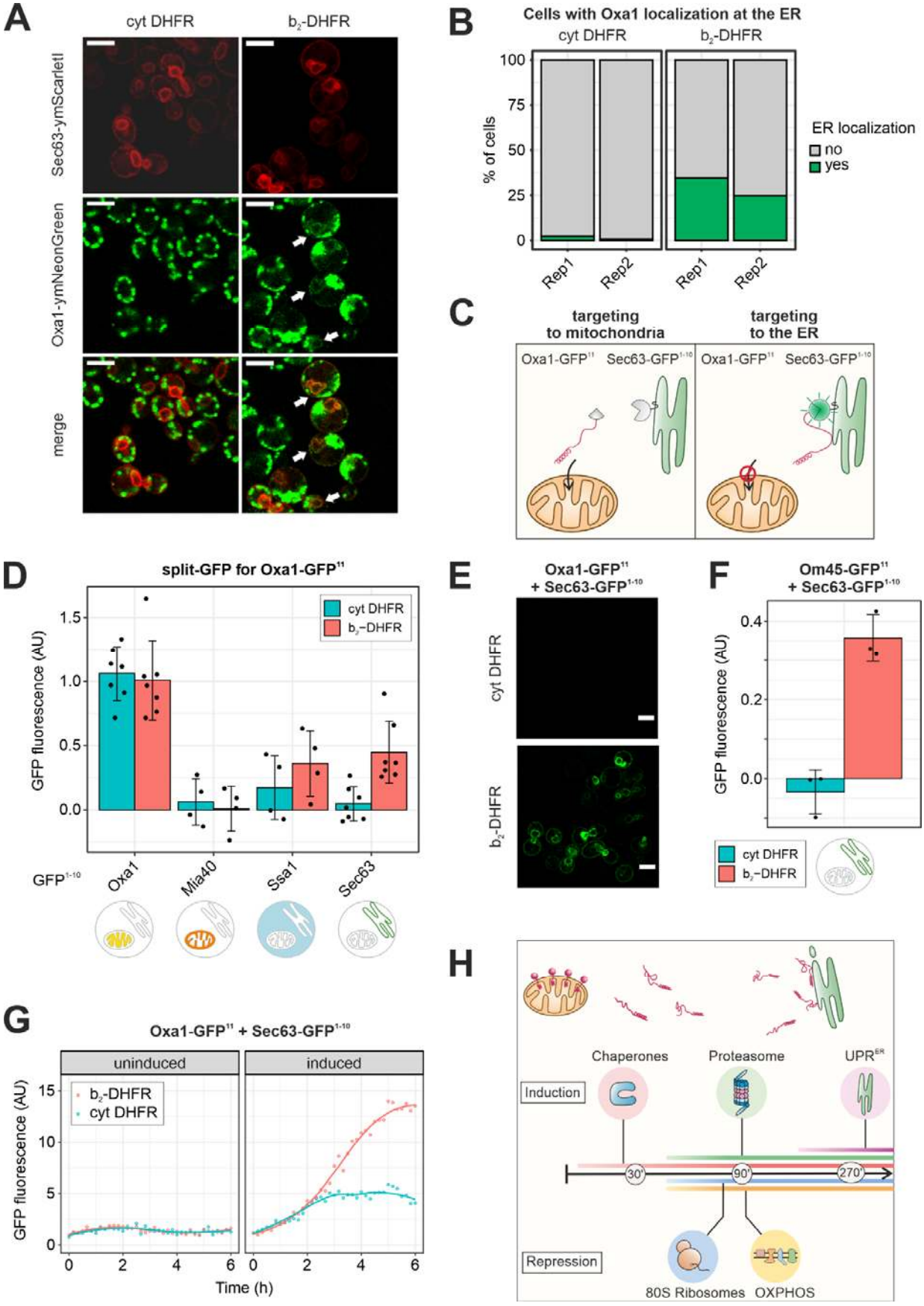

Figure 3. Non-imported mitochondrial membrane proteins localize to the ER. A, The mitochondrial inner membrane protein Oxa1 was genomically tagged with ymNeonGreen, the ER marker Sec63 was tagged with ymScarletI. Confocal fluorescence microscopy was performed after 4.5 h of expression of either b_2-DHFR or cytosolic DHFR. When the clogger was induced, a fraction of Oxa1-ymNeonGreen colocalized with Sec63-ymScarletI. Scale bar, 5 µm. **B,** Quantification of the number of cells from A in which ER localization of Oxa1-ymNeonGreen was observed. **C,** Schematic depiction of the split-GFP strategy to measure ER localization of mitochondrial proteins. **D,** The GFP^{11} fragment was fused to Oxa1 and the GFP^{1-10} fragment was fused to Oxa1, Mia40, Ssa1 or Sec63. b_2-DHFR or cytosolic DHFR were induced for 4.5 h and fluorescence was measured in a platereader. Mean values and standard deviations are shown for n=7 (Oxa1-GFP^{1-10}, Sec63-GFP^{1-10}) or n=4 (Mia40-GFP^{1-10}, Ssa1-GFP^{1-10}) independent biological replicates. **E,** Fluorescence microscopy of cells expressing Oxa1-GFP^{11} and Sec63-GFP^{1-10} and either b_2-DHFR or cytosolic DHFR after 4.5 h of induction. Scale bar, 5 µm. **F,** The GFP^{11} fragment was fused to Om45 and the GFP^{1-10} fragment to Sec63. Clogger expression for 4.5 h evoked an increase in fluorescence (mean values and standard deviations for n=3 independent biological replicates). **G,** Cells expressing Oxa1-GFP^{11} and Sec63-GFP^{1-10} were cultured in lactate medium before either b_2-DHFR or cytosolic DHFR were induced by addition of 0.5 % galactose. Fluorescence was monitored in a Clariostar plate reader every 10 min for n=6 biological replicates. Constitutively expressed ymScarletI was used to normalize for growth and overall translation rates. After around 3 h of induction, elevated split-GFP signals in clogger-expressing cells indicated accumulation of Oxa1 at the ER. **H,** Model for the connection between mitochondrial import block and UPR^{ER} induction. Clogging the mitochondrial translocases leads to accumulation of precursor proteins in the cytosol as well as at the ER surface, which triggers the ER stress response.

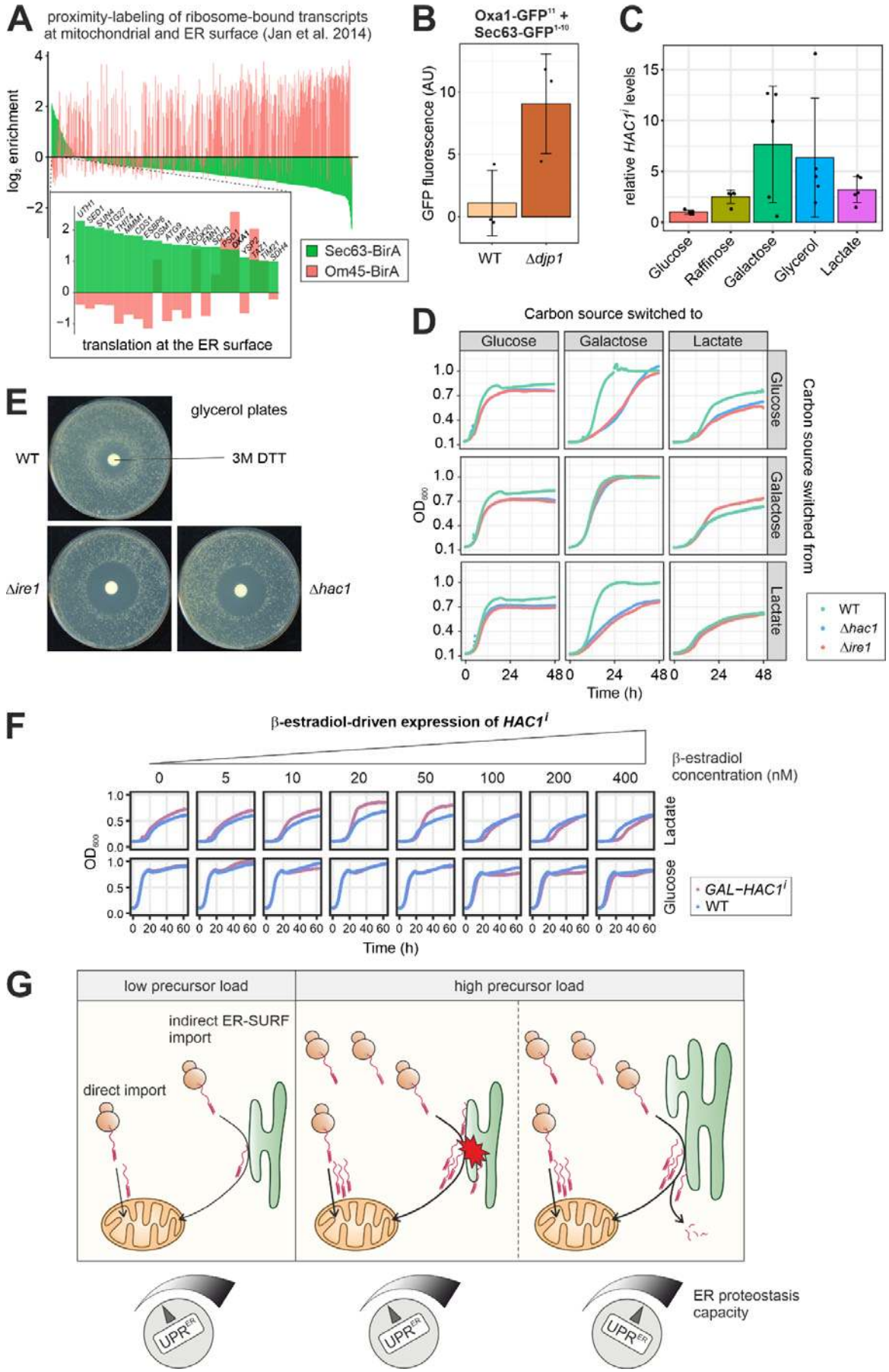

Figure 4. The UPR^{ER} maintains cellular fitness during changes in mitochondrial biogenesis. A, Data from Jan et al. (2014)[59] on the localized translation near the mitochondrial and the ER surface. For all mitochondrial proteins in the dataset, the $\log_2$ enrichment of ribosome-nascent chain complexes at the ER membrane (Sec63-BirA) and the mitochondrial outer membrane (Om45-BirA) over the total ribosomes are shown. While most translated mRNAs localize to the mitochondrial membrane, some transcripts are also or even exclusively enriched near the ER surface (expansion shows genes with more than 2-fold enrichment at the ER). **B,** The ER localization of Oxa1 was determined with the split-GFP assay in wild type and Δ*djp1* cells that were grown to log phase in glucose medium. Oxa1 is trapped at the ER in Δ*djp1*. Mean values and standard deviations from *n*=3 independent biological replicates are shown. **C,** *HAC1* splicing in wild type cells grown to log phase in media with the indicated carbon sources was measured via RT-qPCR. *HAC1*^{i} levels were normalized to total *HAC1* levels. Mean values and standard deviations from *n*=5 independent biological replicates are shown. **D,** Wild type, Δ*ire1* and Δ*hac1* cells were grown to log phase in glucose, galactose and lactate media, washed and switched to glucose, galactose and lactate media in all combinations. Growth was monitored by OD_{600} measurement in a plate reader. Both UPR^{ER}-deficient mutants showed impaired growth when the carbon source was switched to one that promotes higher levels of *HAC1* splicing in wild type cells. **E,** Wild type, Δ*ire1* and Δ*hac1* cells were plated on glycerol and 10 µl of a 3 M solution of the UPR^{ER}-inducing agent dithiotreithol (DTT) were applied on a filter dish in the middle of the plate. Note the ring-like growth of the wild type around the filter dish. **F,** Wild type cells and cells that express *HAC1*^{i} from an estradiol-inducible *GAL* promoter were grown to log phase in glucose medium. They were washed, resuspended in either glucose or lactate medium supplemented with the indicated concentration of estradiol. Ectopic expression of low levels of *HAC1*^{i} result in better growth in lactate, but not in glucose medium. **G,** Schematic model for the role of the UPR^{ER} in mitochondrial protein biogenesis. A fraction of mitochondrial precursor proteins constantly localizes to the ER. Global changes in expression of mitochondrial genes increase the influx of precursors to the ER. Defects in

919 protein import also elevate the levels of ER-resident mitochondrial precursors. In both cases,
920 activation of the UPR^{ER} adjusts the proteostasis capacity of the ER.

921

Supplementary Figures

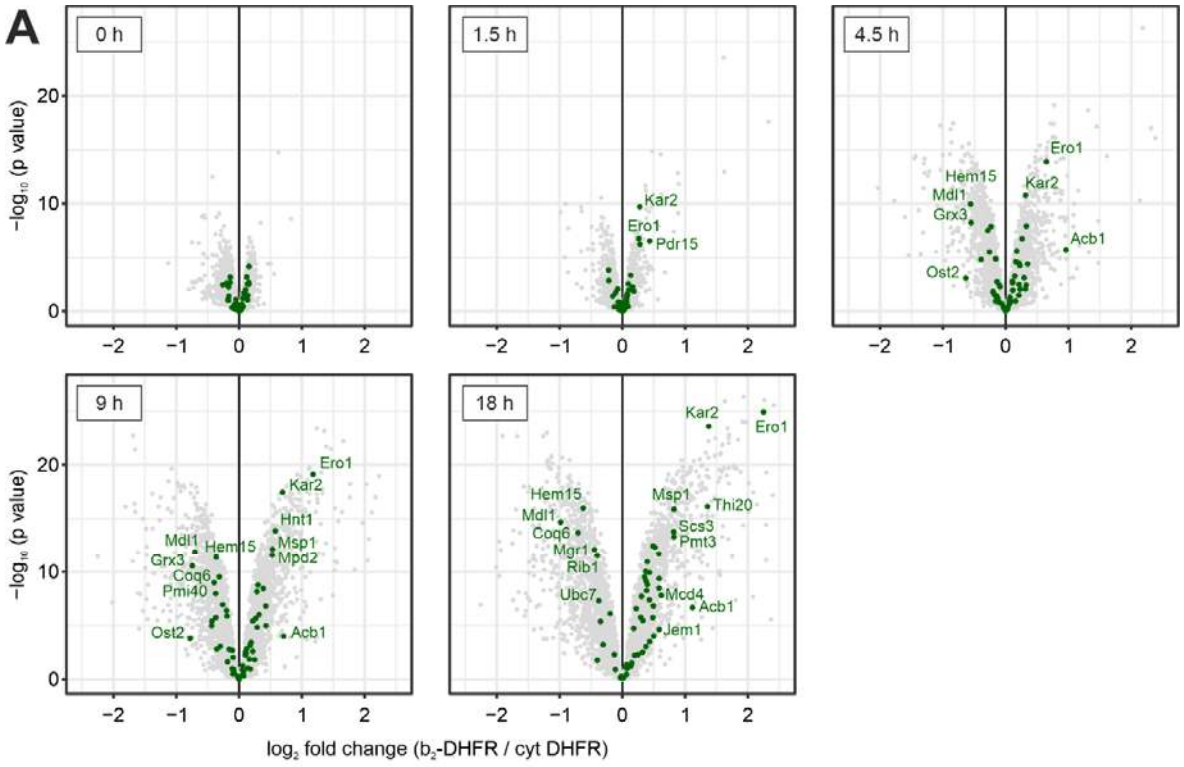

924 **Supplementary Figure 1. Detection of UPR^{ER} induction with mass spectrometry and RT-**
925 **qPCR.**

926 **A,** Protein levels in clogger-expressing versus control cells after different times of induction were
927 measured by quantitative mass spectrometry [28]. Highlighted are proteins which are reported targets
928 of the UPR^{ER} [21]. Data from *n*=3 independent biological replicates are shown. The data for 18 h are
929 the same as shown in Fig. 1E. **B,** The change in translational efficiency after 4.5 h clogger
930 expression was calculated for all genes measured in both the RNA-seq [28] and Ribo-Seq on clogger-
931 expressing cells by dividing the translatome fold change by the transcriptome fold change. **C,**
932 Schematic depiction of the primer-probe combinations used to quantify total *HAC1* as well as
933 spliced *HAC1*^{i} mRNA levels via RT-qPCR. **D,** Wild type, Δ*ire1* and Δ*hac1* cells were grown in
934 presence or absence of 1 µg/ml tunicamycin and *HAC1* and *HAC1*^{i} levels were analyzed with the
935 primer-probe assay shown in C. As expected, *HAC1*^{i} levels increased in wild type cells treated with
936 tunicamyin, but no *HAC1*^{i} was detected in cells lacking *HAC1* or *IRE1*, confirming the specificity
937 of the RT-qPCR assay.

938

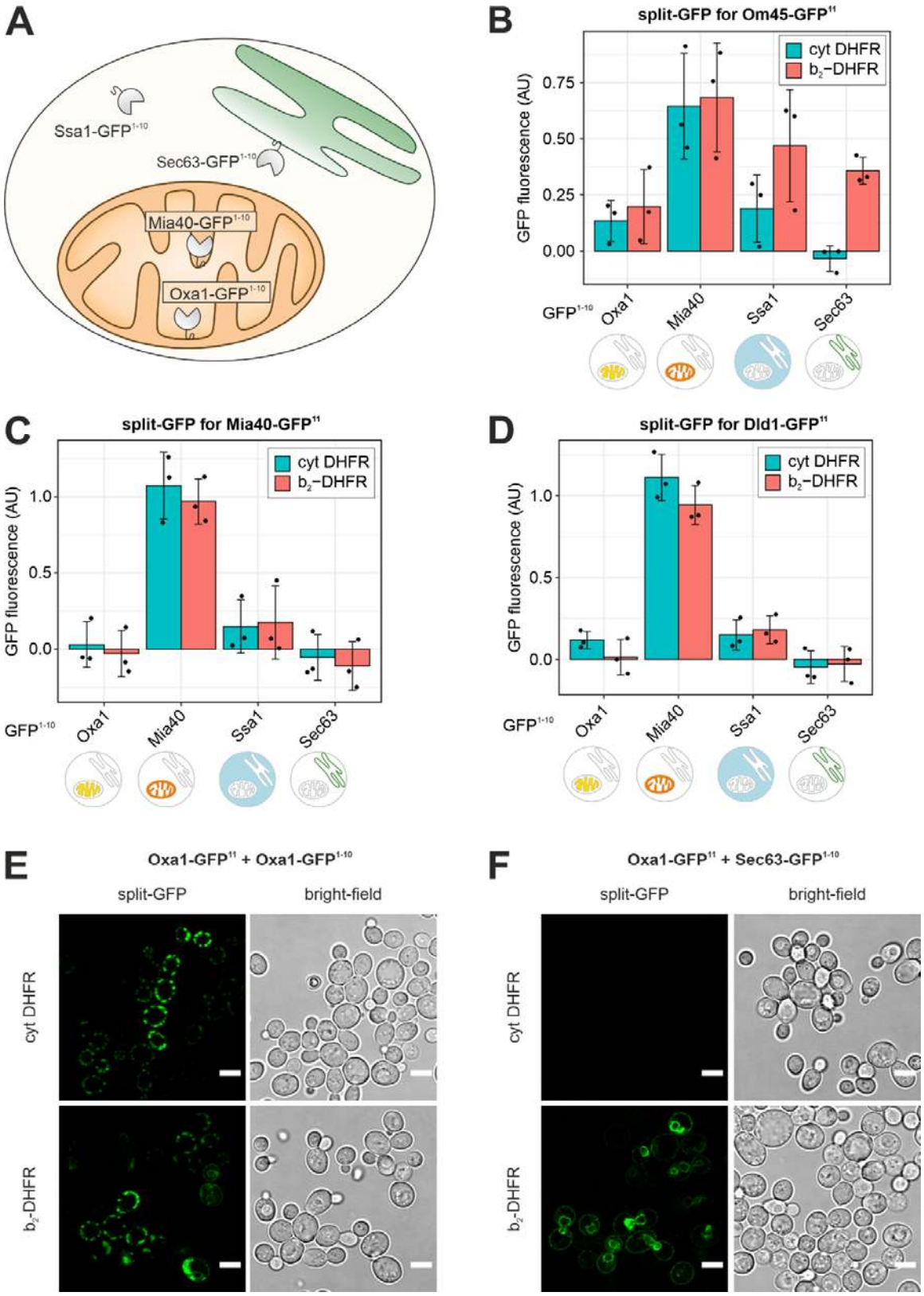

939

940 **Supplementary Figure 2. A split-GFP assay to assess the subcellular localization of**

941 **mitochondrial precursor proteins. A,** The GFP^{11} fragment was fused to Oxa1, Om45, Mia40 and

Dld1, and the GFP$^{1-10}$ reporter was fused to Oxa1 (mitochondrial inner membrane, matrix side), Mia40 (mitochondrial inner membrane, IMS side), Sec63 (ER membrane, cytosolic side) and Ssa1 (cytosol). **B-D,** The split-GFP constructs described in A were co-expressed with b_2-DHFR or cytosolic DHFR and fluorescence was measured with a Clariostar plate reader. Under non-stressed conditions (expression of cytosolic DHFR), the split-GFP signals recapitulated the known localizations of Oxa1, Om45, Mia40 and Dld1. Under mitoprotein-induced stress (b_2-DHFR expression), Om45-GFP^{11} also evoked a fluorescence signal when combined with Sec63-GFP$^{1-10}$ and Ssa1-GFP$^{1-10}$, indicating accumulation at the cytosolic side of the ER membrane. **E,** Fluorescence microscopy of cells expressing Oxa1-GFP^{11} and Oxa1-GFP$^{1-10}$ and either b_2-DHFR or cytosolic DHFR after 4.5 h of induction. Scale bar, 5 µm. **F,** Fluorescence microscopy of cells expressing Oxa1-GFP^{11} and Sec63-GFP$^{1-10}$ and either b_2-DHFR or cytosolic DHFR after 4.5 h of induction. Scale bar, 5 µm. GFP Images are identical to those in Figure 3E.

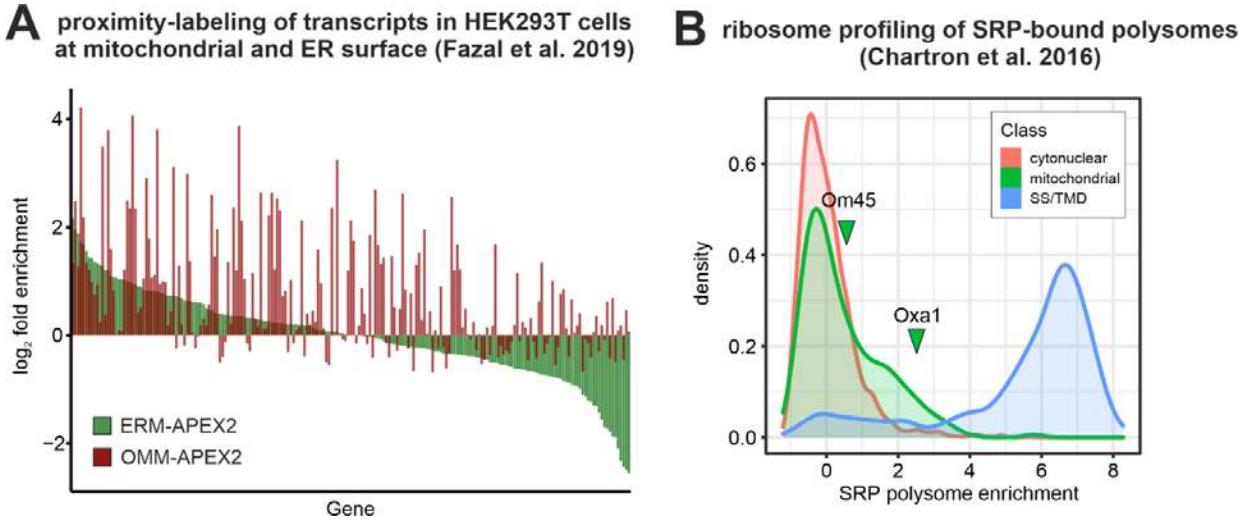

Supplementary Figure 3. Certain mitochondrial proteins are synthesized close to the ER surface and recognized by SRP. A, Data from Fazal et al. (2019)[61] on the subcellular distribution of mRNA in HEK293T cells. The biotin ligase APEX2 was localized to the ER or mitochondria and biotinylated mRNAs were purified and sequenced (APEX-Seq). For all mitochondrial proteins in the dataset, the $\log_2$ enrichment of mRNAs at the ER membrane (ERM-APEX2) and the mitochondrial outer membrane (OMM-APEX2) over the total mRNAs are shown. While most mRNAs localize to the mitochondrial membrane, some transcripts are also enriched near the ER surface. **B,** Data from Chartron et al. (2016)[63] on the SRP-bound translatome in yeast. SRP was immune-purified from cell lysates and the co-isolated ribosome-nascent chains complexes were analyzed by ribosome profiling. The distribution of the $\log_2$ fold enrichment SRP-bound ribosome-nascent chain complexes over total ribosomes is shown for cytonuclear and mitochondrial proteins and proteins that carry a signal sequence or transmembrane domain for ER targeting (SS/TMD). Some mitochondrial proteins, including Oxa1, are bound by SRP.

969 **Supplementary Tables**

970 **Supplementary Table 1.** Yeast strains used in this study.

971 **Supplementary Table 2.** Plasmids used in this study.

972 **Supplementary Table 3.** Primers used in this study.